

Shadowing Effects on Vector Boson Production in $p\text{Pb}$ and $\text{Pb}+\text{Pb}$ Interactions at the LHC

Ramona Vogt

Nuclear Science Division, Lawrence Berkeley National Laboratory, Berkeley, CA
and
Physics Department, University of California, Davis, CA

Outline

- Vector Boson Rapidity Distributions and Cross Sections in pp , $p\text{Pb}$, $\text{Pb}p$, and $\text{Pb}+\text{Pb}$ Interactions
- Study Scale and Model Dependence of Shadowing
- Isospin Important in Quark-Dominated Processes
- Measurements Will Test Shadowing at High Q^2

Proton Parton Distributions

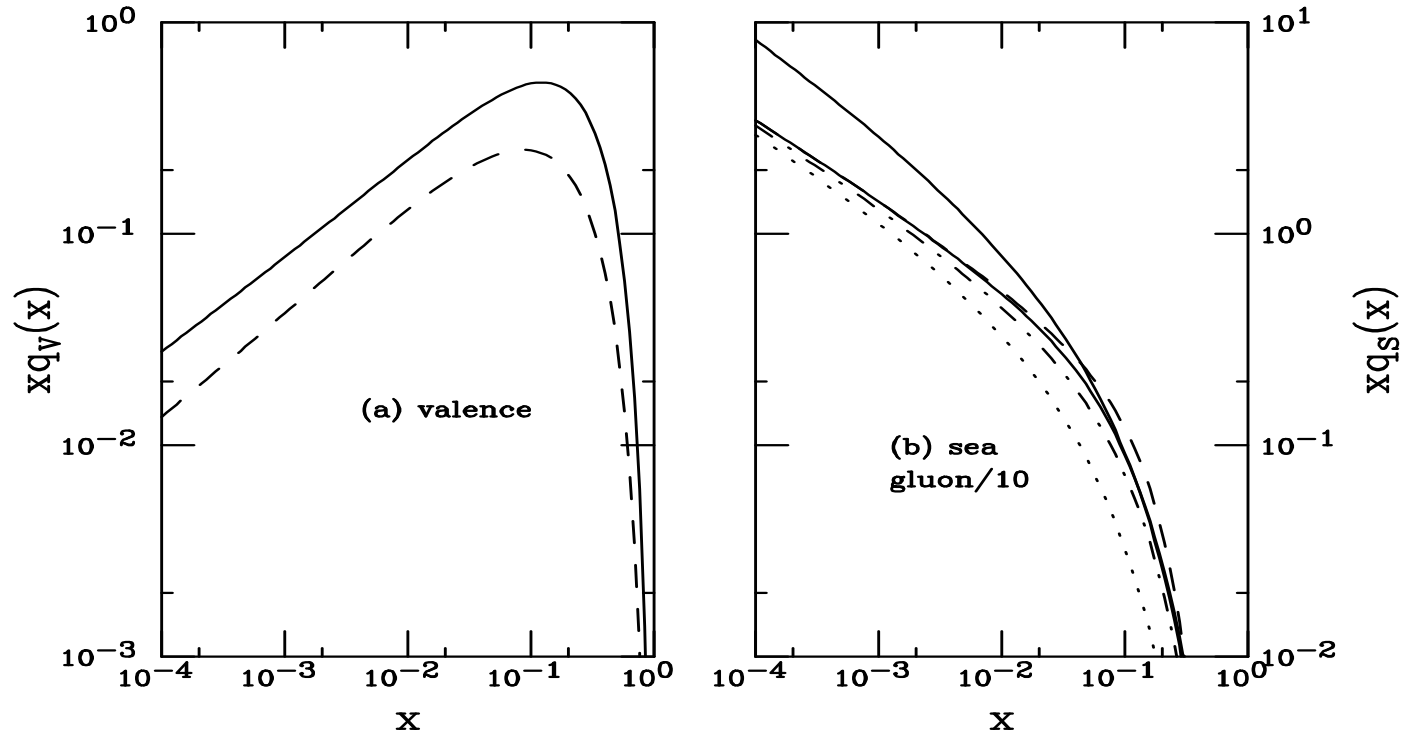


Figure 1: The MRST LO proton parton distribution functions evaluated at $Q = m_Z$. The up (solid) and down (dashed) valence distributions are given in (a) while the up (lower solid), down (dashed), strange (dot-dashed) and charm (dotted) sea quark distributions are shown in (b), along with the gluon distribution (upper solid), reduced by a factor of 10 for comparison. (Phys. Rev. C64 (2001) 044901.)

Shadowing Parameterizations

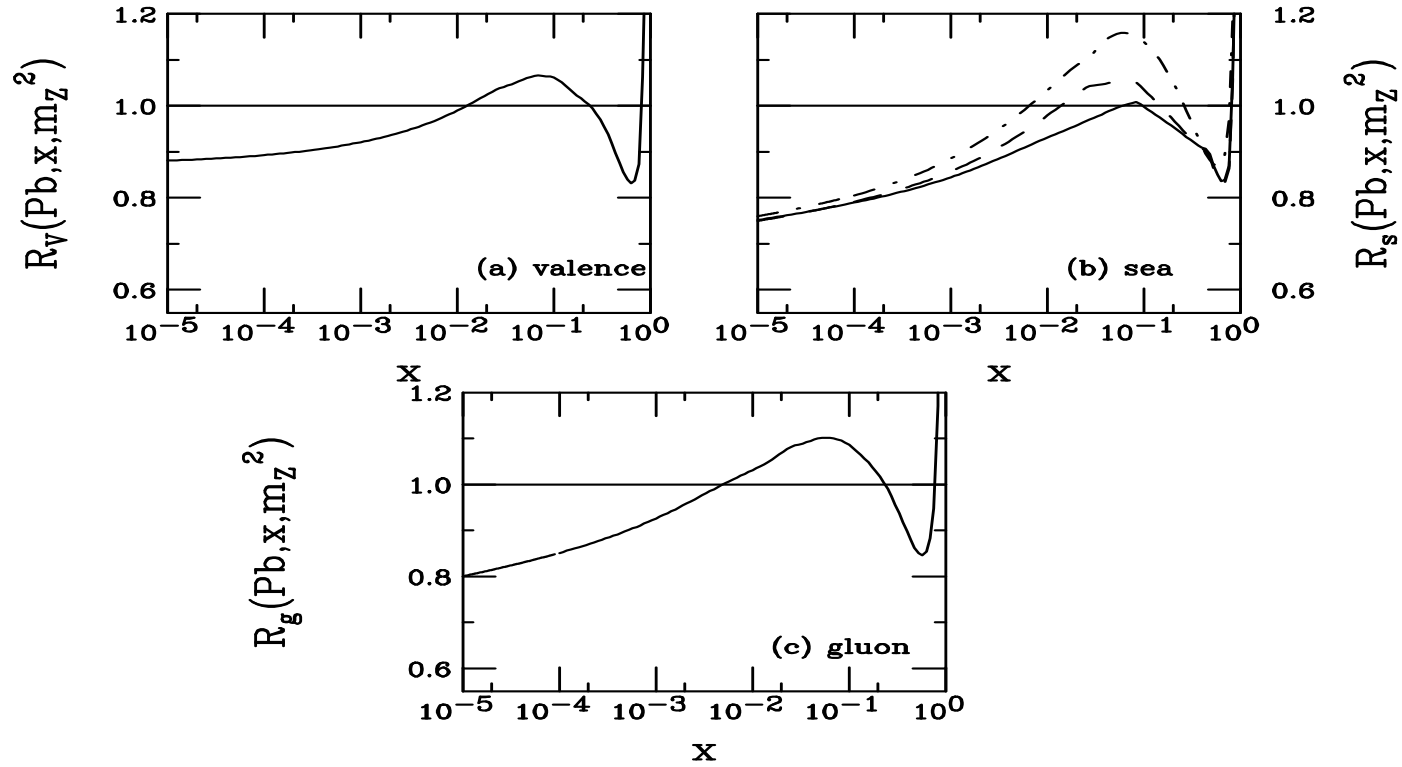


Figure 2: The EKS98 shadowing parameterization evaluated at $Q = m_Z$. Valence shadowing is shown in (a), sea quark shadowing is shown in (b) for $\bar{u} = \bar{d}$ (solid), \bar{s} (dashed) and \bar{c} (dot-dashed), and gluon shadowing is shown in (c).

HKM Nuclear Parton Distributions

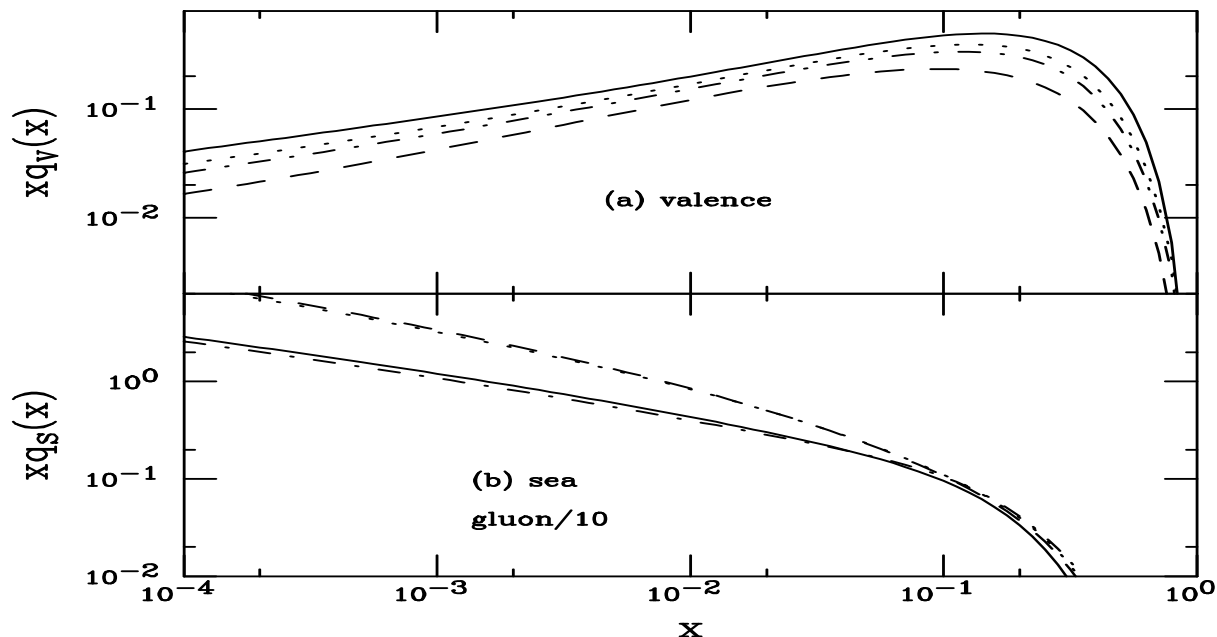


Figure 3: The HKM Pb and proton parton distribution functions evaluated at $Q = m_Z$. The HKM proton distribution is based on the MRST LO parton distribution but modified to have a flavor symmetric ($\bar{u} = \bar{d} = \bar{s}$) sea. In the upper plot, the valence distributions are compared. The proton up and down valence distributions are given in the solid and dashed curves respectively while the Pb up and down valence distributions are given in the dot-dashed and dotted curves. In the lower plot the proton sea (solid) and Pb sea (dot-dashed) distributions are compared, as well as the proton gluon (dashed) and Pb gluon (dotted) distributions. The gluon distributions are reduced by a factor of 10 for comparison.

Shadowing in Gauge Boson Production

Next-to-leading order production of a vector particle with mass m_V at scale Q

$$\begin{aligned} \frac{1}{AB} \frac{d\sigma_{AB}^V}{dy} &= \int dz dz' dx_1 dx_2 dx \delta\left(\frac{m_V^2}{s} - xx_1x_2\right) \delta\left(y - \frac{1}{2} \ln\left(\frac{x_1}{x_2}\right)\right) \\ &\times \left\{ \sum_{i,j \in Q, \bar{Q}} H_{ij}^V C^{ii}(q_i, \bar{q}_j) \Delta_{q\bar{q}}(x) F_{q_i}^A(x_1, Q^2) F_{\bar{q}_j}^B(x_2, Q^2) \right. \\ &\left. + \sum_{i,k \in Q, \bar{Q}} H_{ij}^V C^{if}(q_i, q_k) \Delta_{qq}(x) \left[F_{q_i}^A(x_1, Q^2) F_g^B(x_2, Q^2) + F_g^A(x_1, Q^2) F_{q_j}^B(x_2, Q^2) \right] \right\}, \end{aligned}$$

$$H_{ij}^{Z^0} = \frac{8\pi G_F}{3\sqrt{2}} [(g_V^i)^2 + (g_A^i)^2] \frac{m_Z^2}{s}$$

$$H_{ij}^{W^\pm} = \frac{2\pi G_F m_W^2}{3\sqrt{2} s}$$

$$G_F = 1.16639 \times 10^{-5} \text{ GeV}^{-2}$$

Shadowing effects clearest in rapidity distributions

We use MRST HO central gluon and set $Q = m_V$

To study scale dependence, we also take $Q = m_V/2$ and $2m_V$

Nuclear Parton Distributions

Nuclear parton densities may include spatial dependence

$$\begin{aligned}
 F_i^A(x, Q^2, \vec{r}, z) &= \rho_A(s) S^i(A, x, Q^2, \vec{r}, z) f_i^N(x, Q^2) \\
 F_j^B(x, Q^2, \vec{b} - \vec{r}, z') &= \rho_B(s') S^j(B, x, Q^2, \vec{b} - \vec{r}, z') f_j^N(x, Q^2) \\
 s = \sqrt{r^2 + z^2} \quad \text{and} \quad s' &= \sqrt{|\vec{b} - \vec{r}|^2 + z'^2} \\
 \rho_A(s) &= \rho_0 \frac{1 + \omega(s/R_A)^2}{1 + \exp[(s - R_A)/d]}
 \end{aligned}$$

We use the EKS98 shadowing parameterization for S^i

Spatial dependence can be parameterized according to local density or path length through the nucleus; different x regions may have different dependencies

Normalization of spatial dependence should be such that integration over nuclear density results in measured homogeneous shadowing,

$$\frac{1}{A} \int d^2r dz \rho_A(s) S^i(A, x, Q^2, \vec{r}, z) \equiv S^i(A, x, Q^2)$$

To simplify notation for up and down quarks, we take

$$\begin{aligned}
 S^u(A, x, Q^2) f_u^p(x, Q^2) &= S^{uv}(A, x, Q^2) f_{uv}^p + S^{\bar{u}}(A, x, Q^2) f_u^p \\
 S^d(A, x, Q^2) f_d^p(x, Q^2) &= S^{dv}(A, x, Q^2) f_{dv}^p + S^{\bar{d}}(A, x, Q^2) f_d^p
 \end{aligned}$$

Universal NLO $\mathcal{O}(\alpha_s \alpha^2)$ Corrections to the LO $\mathcal{O}(\alpha^2)$ Cross Sections

$$\begin{aligned} \Delta_{q\bar{q}}(x) = & \delta(1-x) + \frac{\alpha_s}{3\pi} \left\{ -4(1+x) \ln\left(\frac{Q^2}{m^2}\right) - 8(1+x) \ln(1-x) - 4\frac{1+x^2}{1-x} \ln x \right. \\ & \left. + \delta(1-x) \left[6 \ln\left(\frac{Q^2}{m^2}\right) + 8\zeta(2) - 16 \right] + 8\mathcal{D}_0(x) \ln\left(\frac{Q^2}{m^2}\right) + 16\mathcal{D}_1(x) \right\} . \end{aligned}$$

$$\mathcal{D}_i(x) = \left[\frac{\ln(1-x)}{1-x} \right]_+ = \delta(1-x) \frac{\ln^{i+1}(1-x)}{i+1} + \theta(1-\delta-x) \frac{\ln^i(1-x)}{1-x}$$

$$\int_a^1 dx f(x) \left[\frac{\ln(1-x)}{1-x} \right]_+ = \int_a^1 dx \frac{f(x) - f(1)}{1-x} \ln(1-x) + \frac{1}{2} f(1) \ln^2(1-x)$$

$$\Delta_{qg}(x) = \frac{\alpha_s}{8\pi} \left\{ 2(1+2x^2-2x) \ln\left(\frac{(1-x)^2 Q^2}{xm^2}\right) + 1 - 7x^2 + 6x \right\} .$$

$$\begin{aligned} (g_V^i)^2 + (g_A^i)^2 &= (1/8)(1 - 4|e_i|x_W + 8e_i^2 x_W^2) \\ x_W &= \sin^2 \theta_W = 1 - m_W^2/m_Z^2 \end{aligned}$$

K Factors in pp at 5.5 TeV

K factors calculated for MRST HO distributions in both LO and NLO contributions
Rise in K indicates where gq contribution becomes important

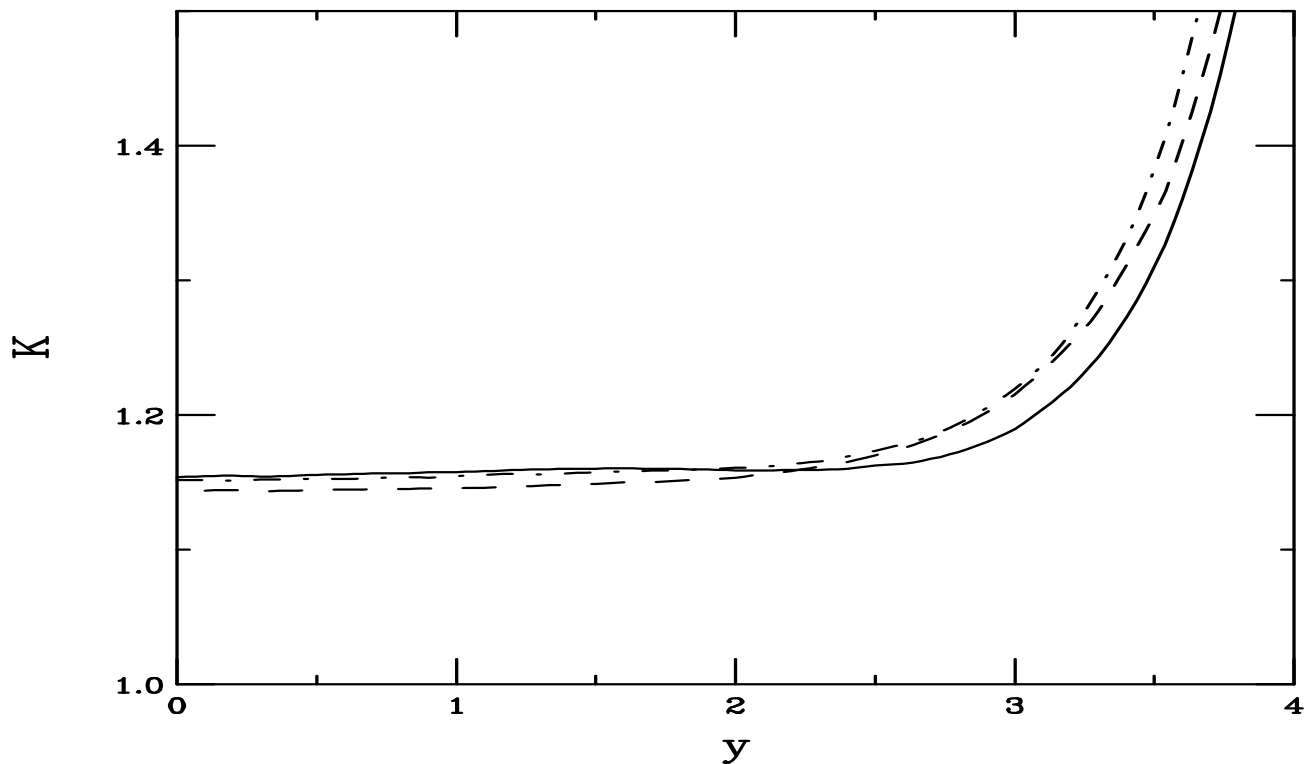


Figure 4: The K factors for W^+ (solid), W^- (dashed), and Z^0 (dot-dashed) production are shown for pp interactions at 5.5 TeV.

Dependence of Z^0 K Factor on Scale

$Q = m_V/2$, log corrections have opposite sign relative to other NLO corrections, decreases K at central y

$Q = 2m_V$, log corrections enhance NLO corrections, increasing K at $y \sim 0$

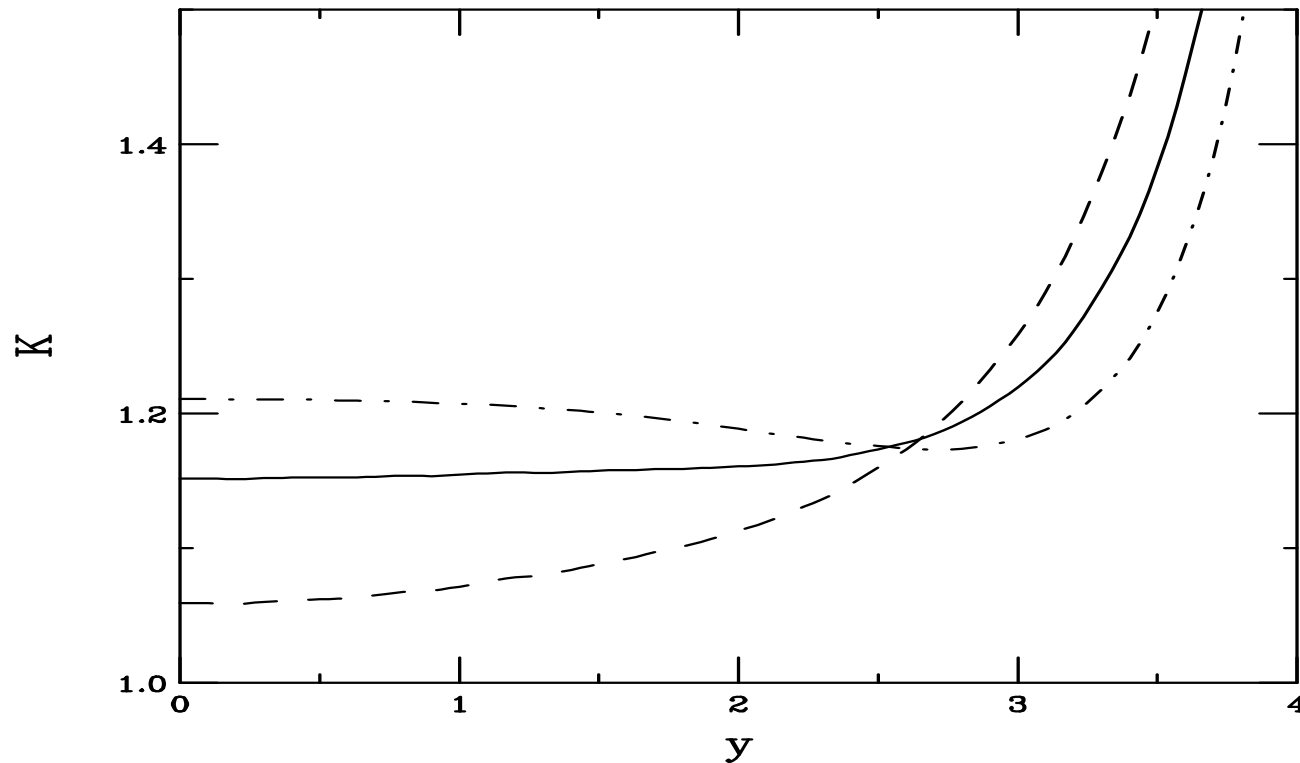


Figure 5: The Z^0 K factors as a function of scale. The results with $Q = m_V$ (solid), $m_V/2$ (dashed), and $2m_V$ (dot-dashed) are shown.

Z^0 Production: Convolution of Shadowing Functions with Parton Densities

$q\bar{q} \rightarrow Z^0 X$

$$\begin{aligned}
& \sum_{i,j \in Q\bar{Q}} S^i(A, x_1) S^j(B, x_2) f_{q_i}^N(x_1, Q^2) f_{\bar{q}_j}^N(x_2, Q^2) C^{ii}(q_i, \bar{q}_j) [(g_V^i)^2 + (g_A^i)^2] \\
&= \frac{1}{8} \left[1 - \frac{8}{3} x_W + \frac{32}{9} x_W^2 \right] \left(S^u(A, x_1) S^{\bar{u}}(B, x_2) \{ Z_A f_u^p(x_1, Q^2) + N_A f_u^n(x_1, Q^2) \} \right. \\
&\quad \times \left. \{ Z_B f_u^p(x_2, Q^2) + N_B f_u^n(x_2, Q^2) \} + 2ABS^c(A, x_1) S^{\bar{c}}(B, x_2) f_c^p(x_1, Q^2) f_c^p(x_2, Q^2) \right) \\
&\quad + \frac{1}{8} \left[1 - \frac{4}{3} x_W + \frac{8}{9} x_W^2 \right] \left(S^d(A, x_1) S^{\bar{d}}(B, x_2) \{ Z_A f_d^p(x_1, Q^2) + N_A f_d^n(x_1, Q^2) \} \right. \\
&\quad \times \left. \{ Z_B f_d^p(x_2, Q^2) + N_B f_d^n(x_2, Q^2) \} + 2ABS^s(A, x_1) S^{\bar{s}}(B, x_2) f_s^p(x_1, Q^2) f_s^p(x_2, Q^2) \right) \\
&\quad + [x_1 \leftrightarrow x_2, A \leftrightarrow B] .
\end{aligned}$$

$q(\bar{q})g \rightarrow Z^0 X$

$$\begin{aligned}
& \sum_{i,k \in Q\bar{Q}} \left(S^i(A, x_1) S^g(B, x_2) f_{q_i}^N(x_1, Q^2) f_g^N(x_2, Q^2) + [x_1 \leftrightarrow x_2, A \leftrightarrow B] \right) C^{if}(q_i, q_k) [(g_V^i)^2 + (g_A^i)^2] \\
&= BS^g(B, x_2) f_g^p(x_2, Q^2) \left\{ \frac{1}{8} \left[1 - \frac{8}{3} x_W + \frac{32}{9} x_W^2 \right] \left(S^u(A, x_1) \{ Z_A f_u^p(x_1, Q^2) + N_A f_u^n(x_1, Q^2) \} \right. \right. \\
&\quad \left. \left. + S^{\bar{u}}(A, x_1) \{ Z_B f_u^p(x_2, Q^2) + N_B f_u^n(x_2, Q^2) \} + 2AS^c(A, x_1) f_c^p(x_1, Q^2) \right) \right. \\
&\quad \left. + \frac{1}{8} \left[1 - \frac{4}{3} x_W + \frac{8}{9} x_W^2 \right] \left(S^d(A, x_1) \{ Z_A f_d^p(x_1, Q^2) + N_A f_d^n(x_1, Q^2) \} \right. \right. \\
&\quad \left. \left. + S^{\bar{d}}(A, x_1) \{ Z_B f_d^p(x_2, Q^2) + N_B f_d^n(x_2, Q^2) \} + 2AS^s(A, x_1) f_s^p(x_1, Q^2) \right) \right\} \\
&\quad + [x_1 \leftrightarrow x_2, A \leftrightarrow B] .
\end{aligned}$$

Z^0 Distributions in pp Collisions at 5.5 and 14 TeV

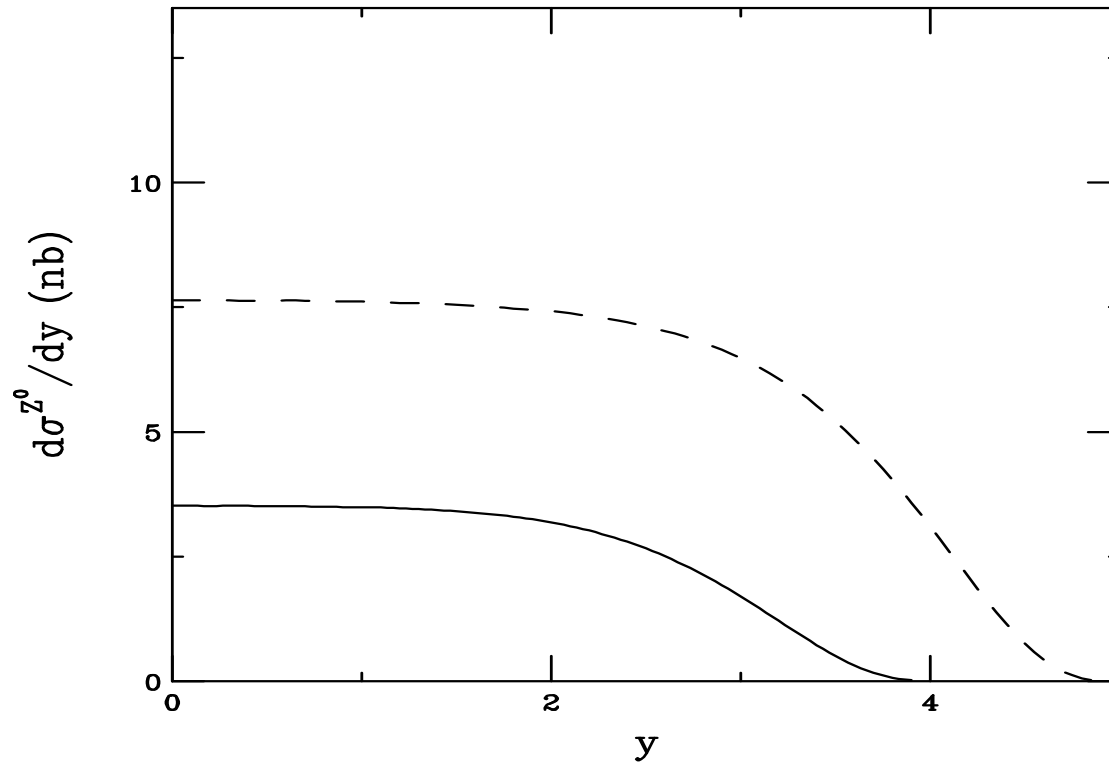


Figure 6: The Z^0 rapidity distributions in pp collisions at 5.5 (solid) and 14 TeV (dashed), calculated with the MRST HO distributions.

Z^0 Distributions in Pb+Pb Collisions at 5.5 TeV

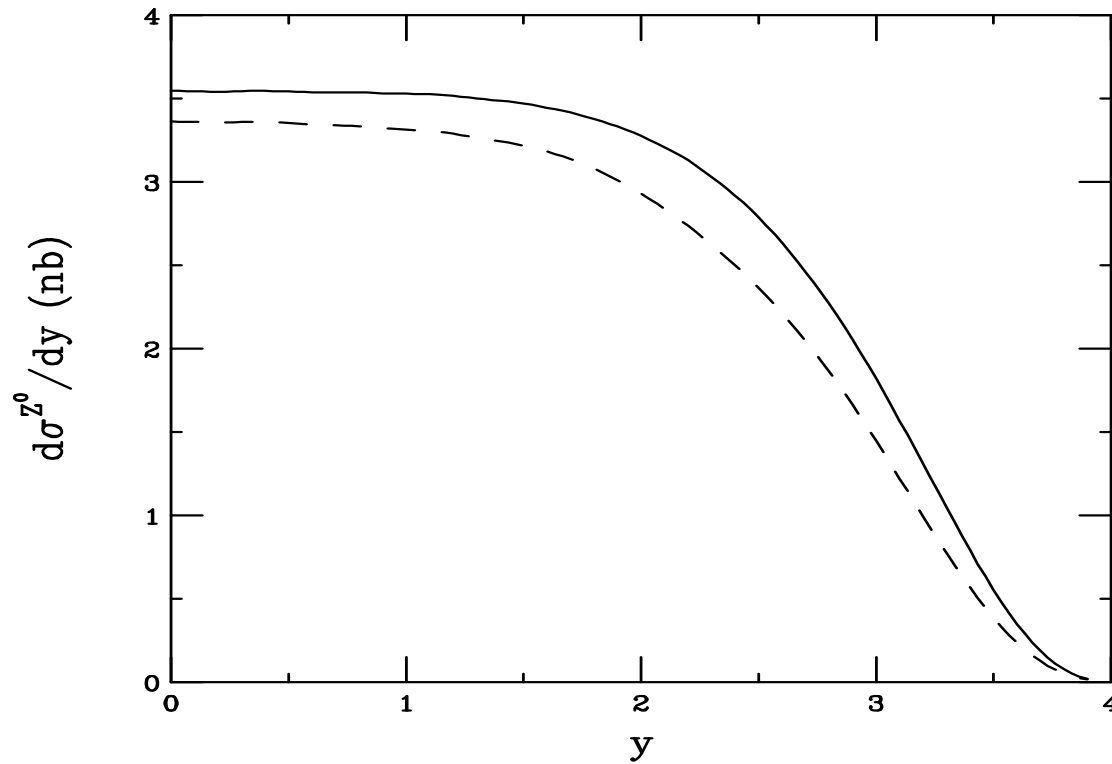


Figure 7: The Z^0 rapidity distributions in Pb+Pb collisions at 5.5 TeV, without (solid) and with EKS98 shadowing (dashed), calculated with the MRST HO distributions.

Effect Independent of Order of Calculation

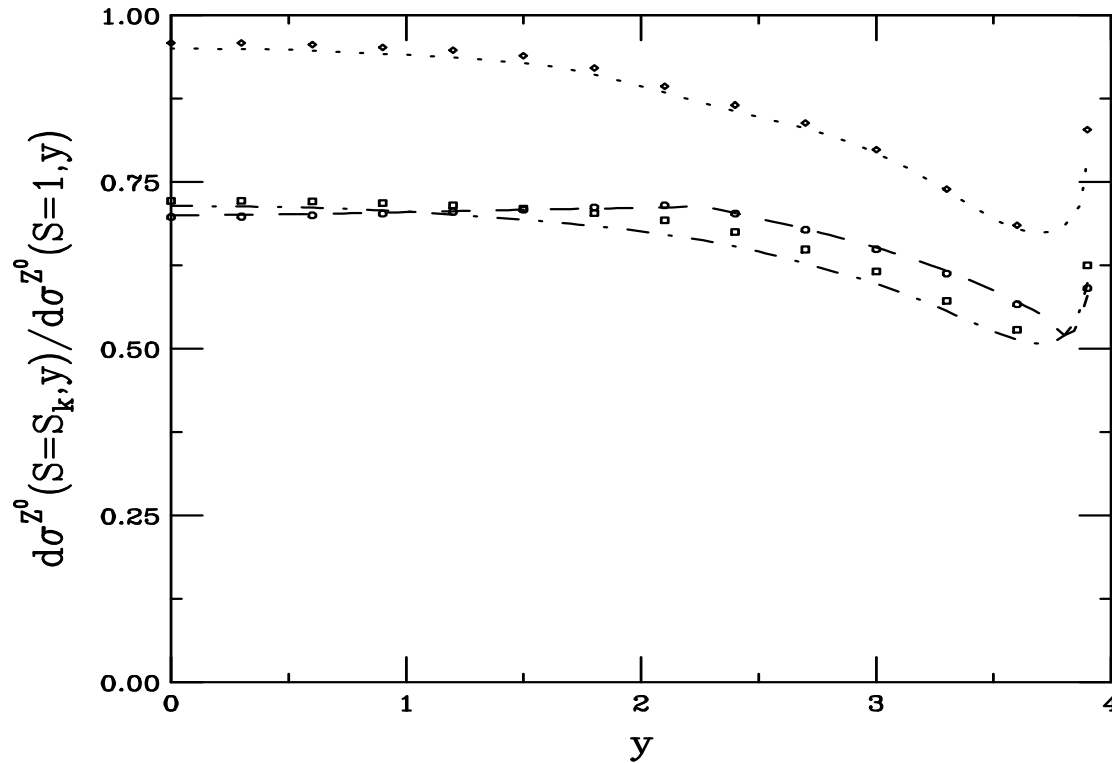


Figure 8: The Z^0 shadowing results at LO and NLO are compared. The NLO results are given in the dashed, HPC, dot-dashed, Eskola, and dotted, EKS98, lines. The LO shadowing ratios for HPC, circles, Eskola, squares, and EKS98, diamonds, are also shown. (Phys. Rev. C64 (2001) 044901.)

Z^0 Shadowing as a Function of Centrality

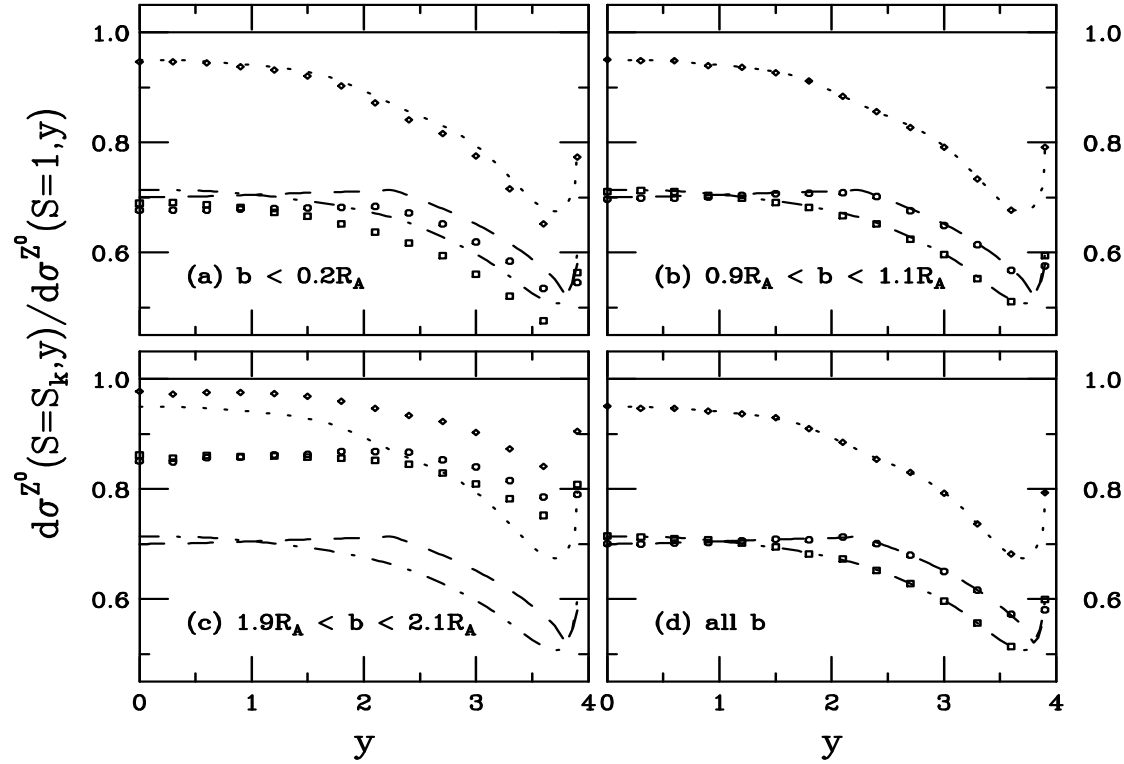


Figure 9: The Z^0 rapidity distributions, relative to no shadowing for Pb+Pb collisions. Central, $b < 0.2R_A$, semi-central, $0.9R_A < b < 1.1R_A$, peripheral, $1.9R_A < b < 2.1R_A$ impact parameters are shown along with the integral over all b . The b -independent results are given in the dashed, HPC, dot-dashed, Eskola, and dotted, EKS98, lines. The b -dependent ratios for HPC, circles, Eskola, squares, and EKS98, diamonds, are also shown. (Phys. Rev. C64 (2001) 044901.)

Comparison to No Shadowing Scenario Unrealistic

For results shown so far, we have assumed pp comparison data at the same energy as Pb+Pb, 5.5 TeV/nucleon

Only gluon-dominated processes such as quarkonium and heavy flavor production will be straightforward to compare at the same energy—no isospin effects

First, best comparison data most likely from pp at $\sqrt{s} = 14$ TeV, 2.5 times larger than Pb+Pb

Different x regions for different energies

Rapidity distributions broader in pp e.g. $|y_{Z^0}| \leq 4$ in Pb+Pb and $|y_{Z^0}| \leq 5$ in pp

We compare the predicted Z^0 distributions in Pb+Pb at 5.5 TeV/nucleon to pp at 14 TeV

Z^0 Ratios to pp at 14 TeV

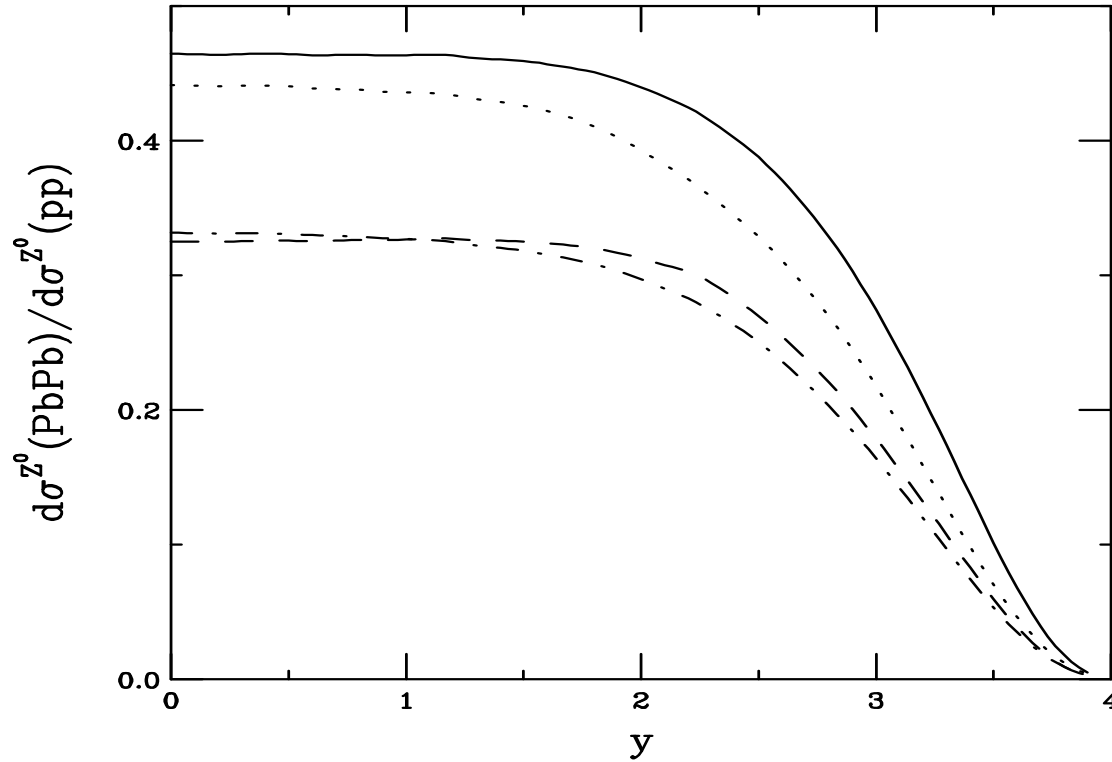


Figure 10: The ratios of the Z^0 rapidity distributions in Pb+Pb collisions relative to pp collisions, calculated with the MRST HO distributions. The solid curve is the ratio without shadowing. The homogeneous shadowing results are given in the dashed, S_1 , dot-dashed, S_2 , and dotted, S_3 , lines. (Phys. Rev. C64 (2001) 044901.)

Contributions from Z^0 Decays in the Continuum Mostly $q\bar{q}$ for $p_T < 15$ GeV, Lower Mass Lepton Pairs Dominated by $(q + \bar{q})g$

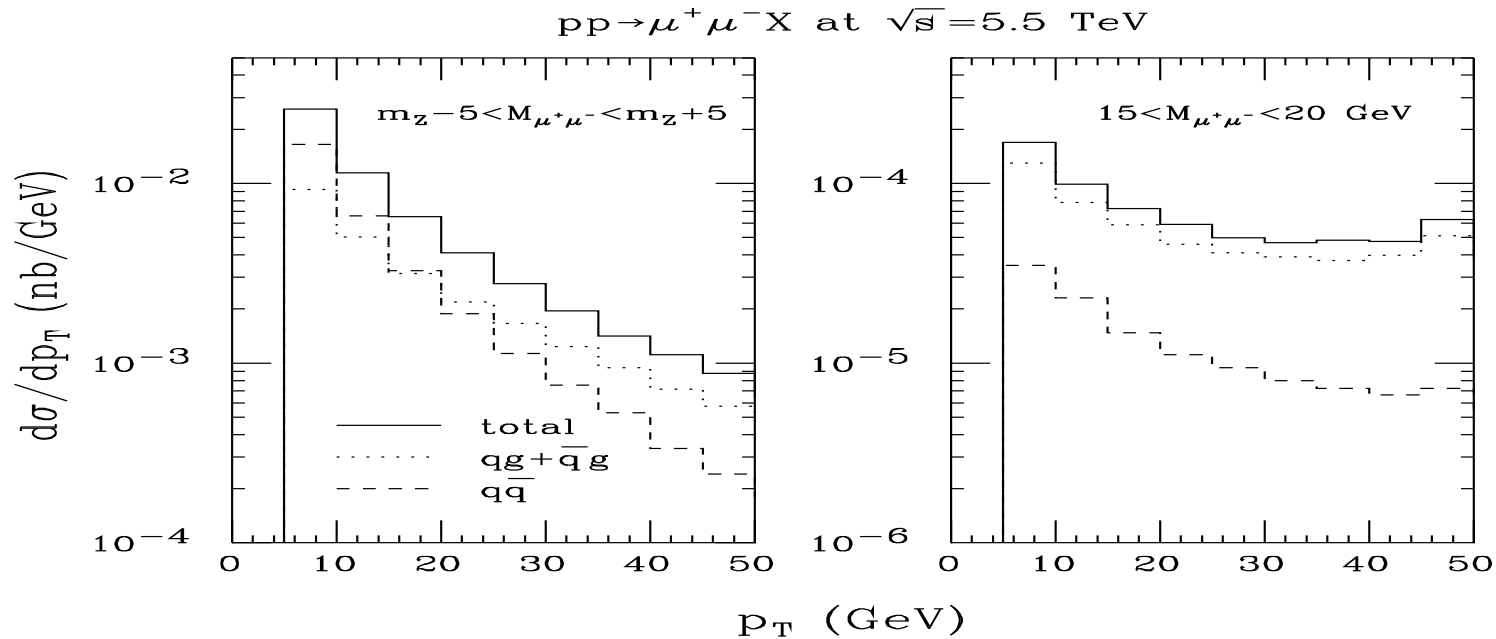


Figure 11: The p_T distribution of dileptons around the mass of the Z^0 , $m_Z \pm 5$ GeV, (left hand side) and for $15 < M < 20$ GeV (right hand side). The distributions are calculated in pp collisions at 5.5 TeV, the same as the Pb+Pb energy. The dotted histogram is the $(q + \bar{q})g$ contribution, the dashed is the $q\bar{q}$ contribution, and the solid histogram is their sum. (Nucl. Phys. B492 (1997) 301.)

Z^0 Distributions in Pbp and pPb Collisions at 5.5 TeV

Small isospin effects on Z^0 production

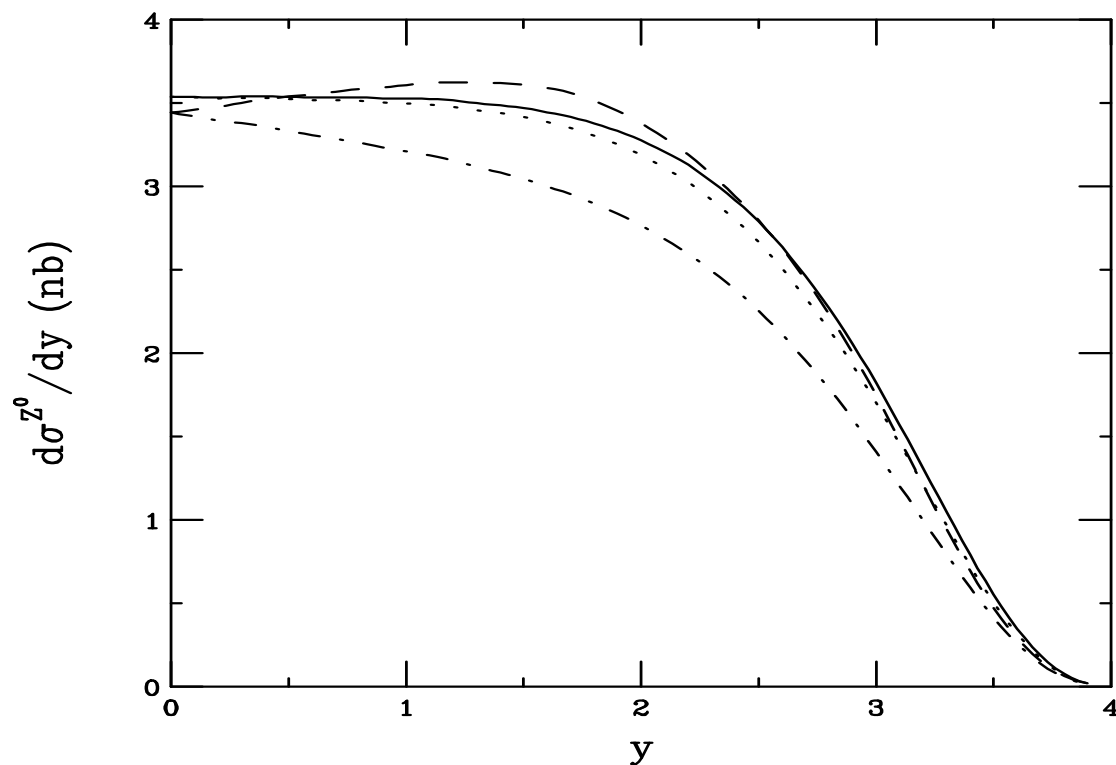


Figure 12: The Z^0 rapidity distributions in Pbp and pPb collisions at 5.5 TeV, calculated with the MRST HO distributions. The solid and dashed curves show the results without and with shadowing respectively with the Pb nucleus coming from the left. The dotted and dash-dotted curves give the results without and with shadowing for the proton coming from the left.

Shadowing Effects on Z^0 Production in Pbp and pPb Collisions at 5.5 TeV

In Pbp collisions, x_1 is in nucleus, x_1 increases with y into antishadowing and Fermi motion region, ratio increases

In pPb collisions, x_2 in nucleus, goes into shadowing region, ratio decreases

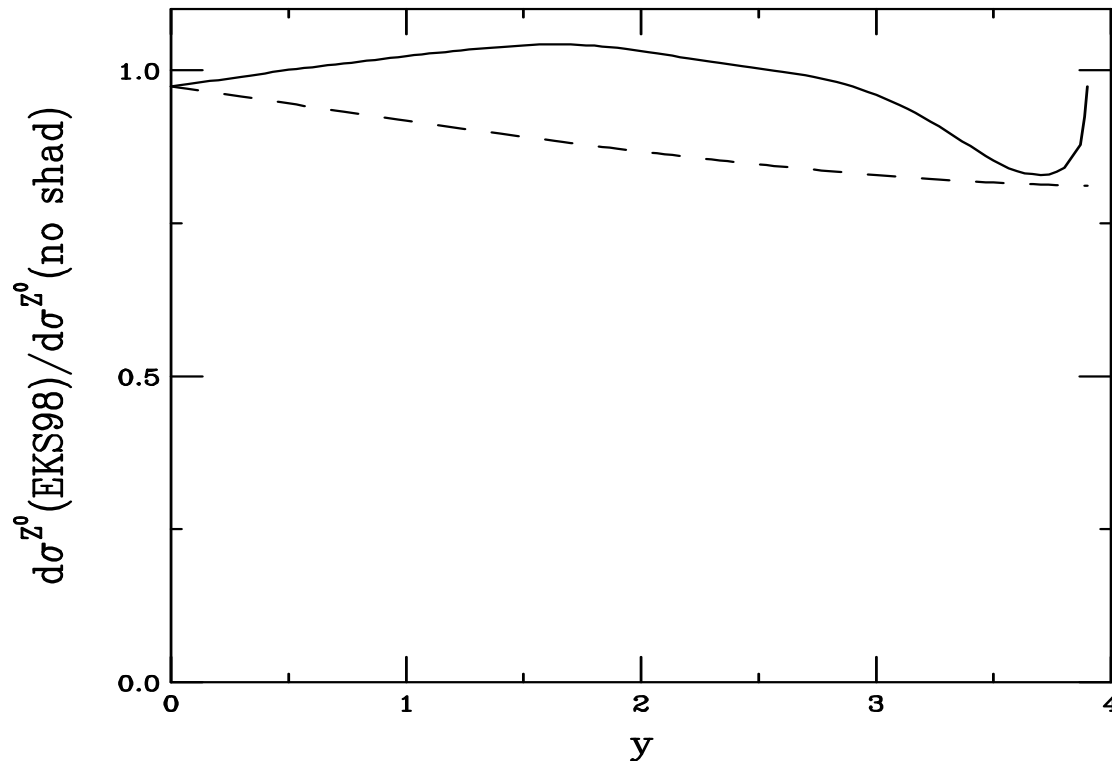


Figure 13: Ratios of shadowed to unshadowed Z^0 rapidity distributions in Pbp (solid) and pPb (dashed) collisions at 5.5 TeV.

Model Dependence of Shadowing on Z^0 Production in Pb p Collisions

Compare EKS98, HPC, and HKM (LO only)

Stronger HKM antishadowing at large y because of increasing q_S with x_1 and weaker q_V shadowing

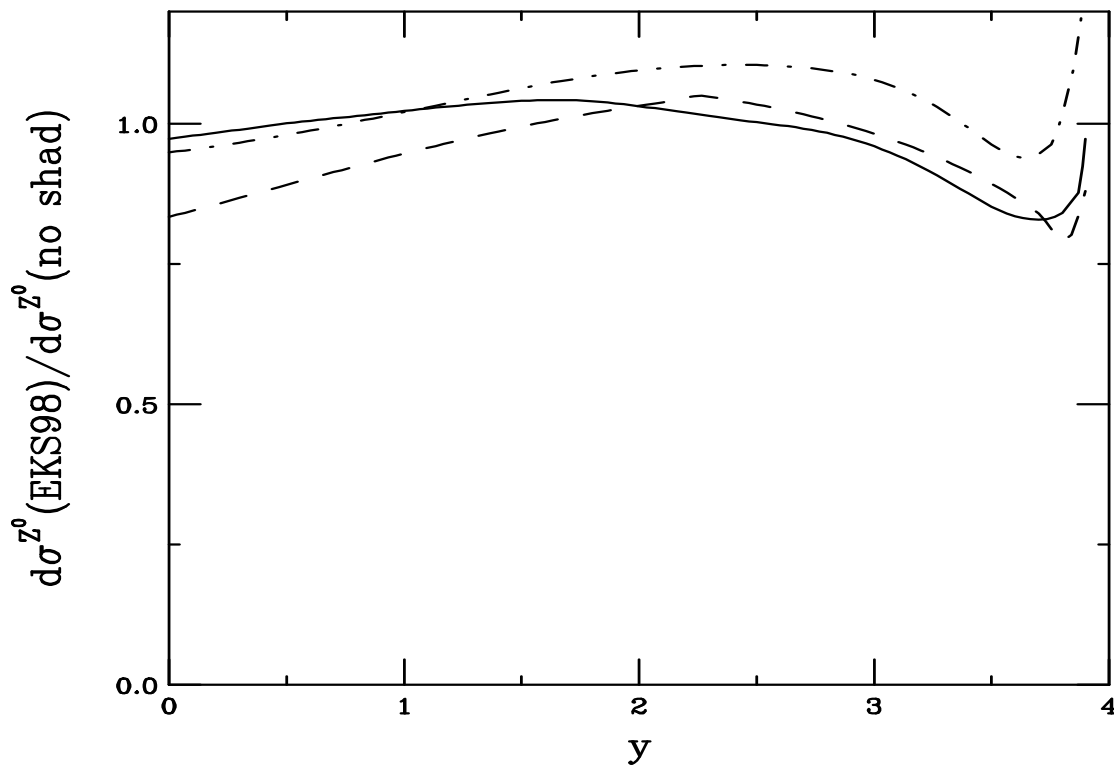


Figure 14: Ratios of shadowed to unshadowed Z^0 rapidity distributions in Pb p collisions at 5.5 TeV using the EKS98 (solid), HPC (dashed) and HKM (dot-dashed) shadowing parameterizations.

Model Dependence of Shadowing on Z^0 Production in p Pb Collisions

HKM shadowing almost independent of x_2 due to weaker sea quark shadowing
HPC has stronger shadowing at low x_2 because it has no Q^2 evolution

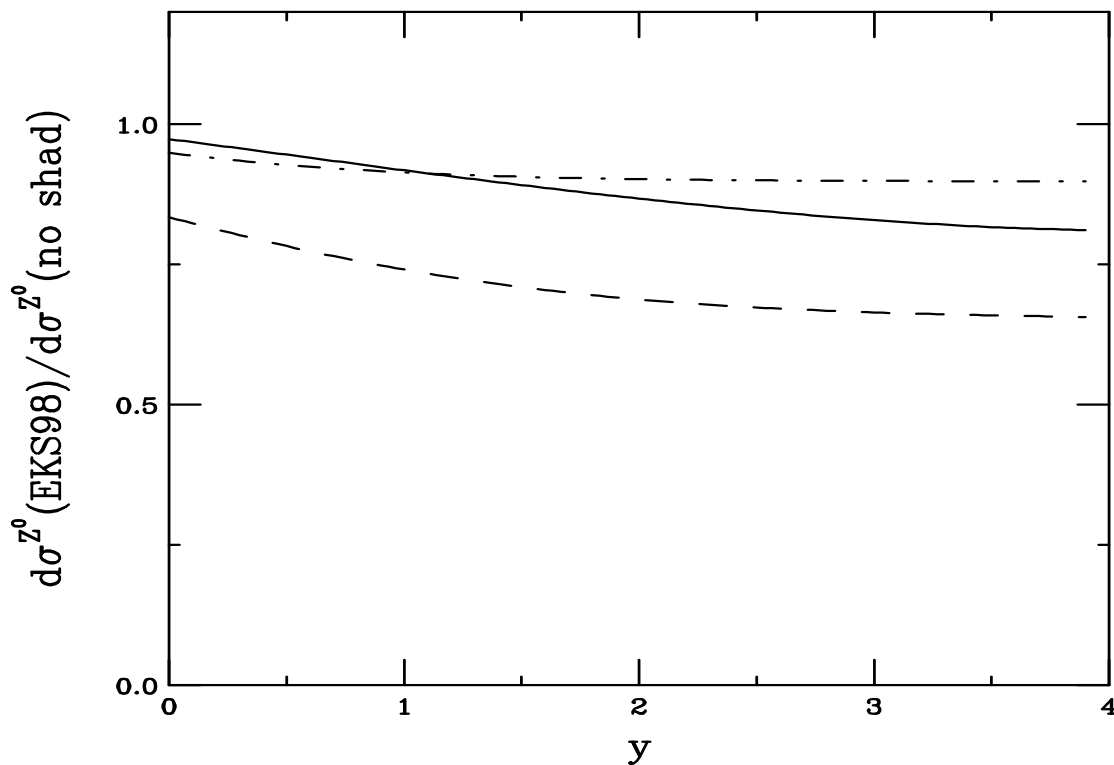


Figure 15: Ratios of shadowed to unshadowed Z^0 rapidity distributions in p Pb collisions at 5.5 TeV using the EKS98 (solid), HPC (dashed) and HKM (dot-dashed) shadowing parameterizations.

Scale Dependence of Shadowing on Z^0 Production in Pb Collisions

Results above $Q = 2m_V$ are unreliable because EKS98 only evolved to 100 GeV
Decreasing scale increases shadowing because evolution reduced

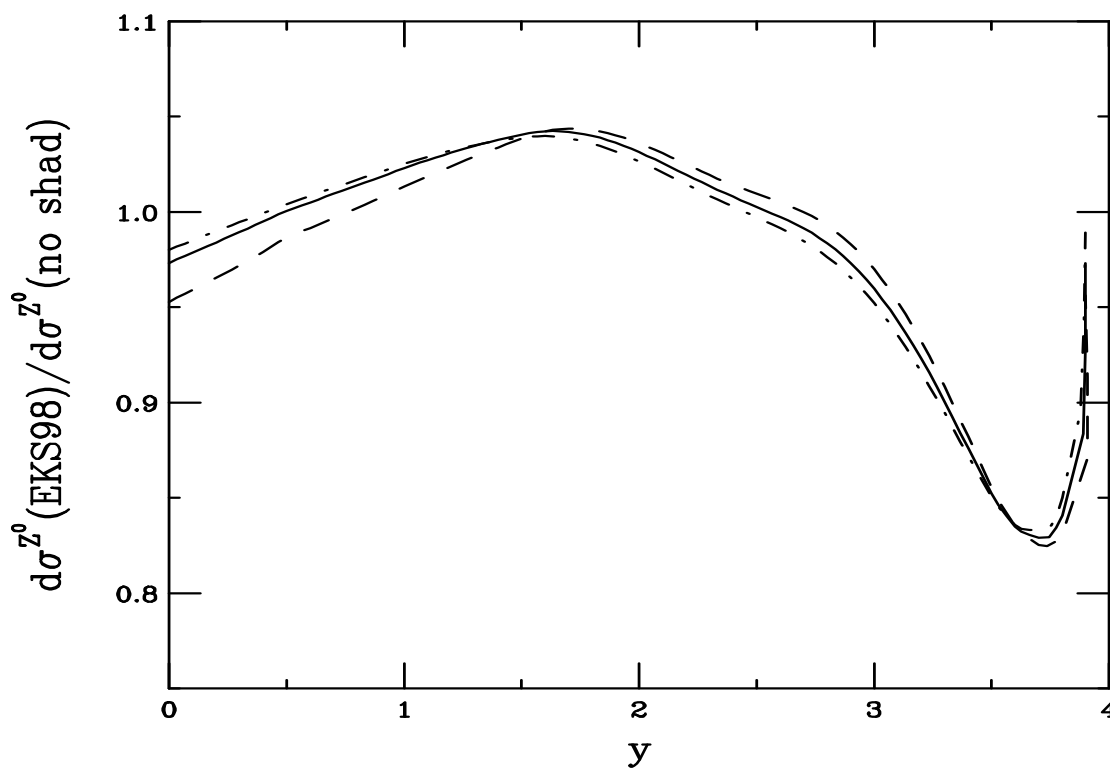


Figure 16: Ratios of shadowed to unshadowed Z^0 rapidity distributions in Pb

collisions at 5.5 TeV using the EKS98 parameterization. The curves show $Q = m_V$ (solid), $m_V/2$ (dashed) and $2m_V$.

Scale Dependence of Shadowing on Z^0 Production in $p\text{Pb}$ Collisions

Evolution of shadowing stronger when Pb is target because shadowing affects sea quarks more strongly at low x_2

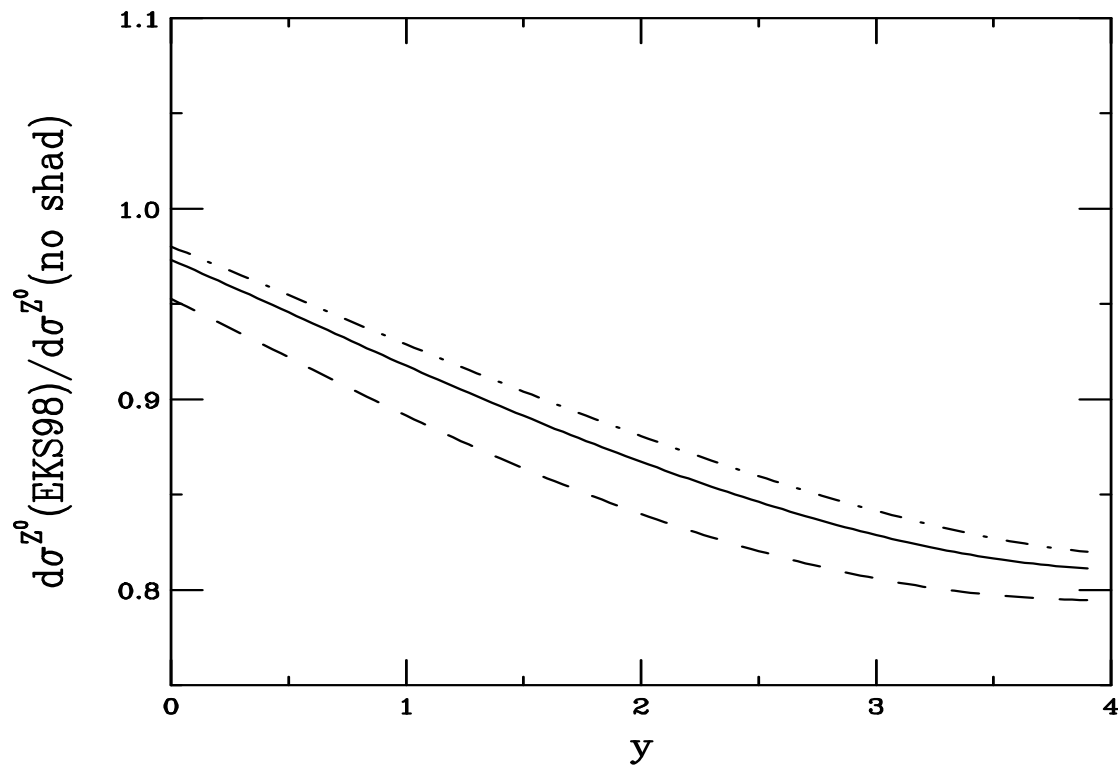


Figure 17: Ratios of shadowed to unshadowed Z^0 rapidity distributions in $p\text{Pb}$ collisions at 5.5 TeV using the EKS98 parameterization. The curves show $Q = m_V$ (solid), $m_V/2$ (dashed) and $2m_V$.

Z^0 Production Ratios Pbp/pp and pPb/pp at 5.5 TeV

Ratios without shadowing show isospin effect, small for Z^0

Thus ratios with shadowing look like shadowed/unshadowed ratios

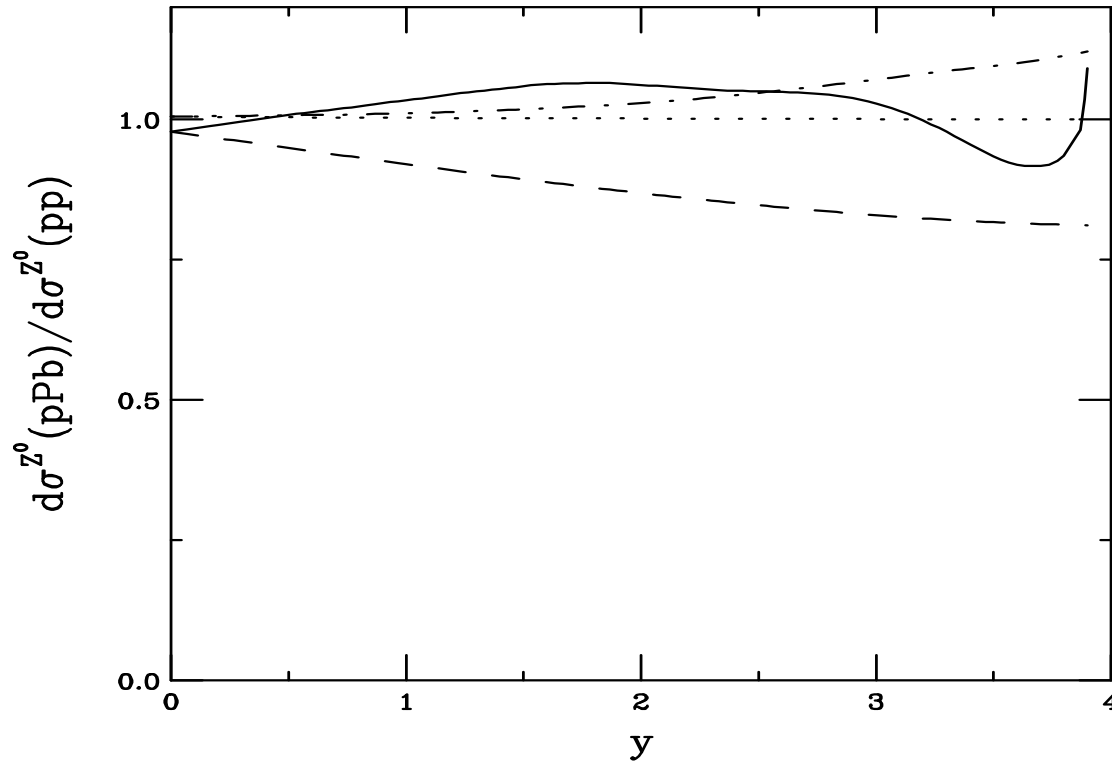


Figure 18: The ratios of Pbp/pp with (solid) and without (dot-dashed) shadowing and pPb/pp with (dashed) and without (dotted) shadowing at 5.5 TeV.

Z^0 Cross Sections

Rapidity	σ (nb)	σ (nb)	σ (no shad) (nb)	σ (EKS98) (nb)
	<i>pp</i> (14 TeV)	<i>pp</i> (5.5 TeV)	Pb+Pb (5.5 TeV)	
$y < 2.4$	18.09	8.10	8.23	7.62
$y < 1$	7.63	3.51	3.54	3.35
$2.4 < y < 4$	9.20	2.01	2.14	1.72

Rapidity	σ (no shad) (nb)	σ (EKS98) (nb)	σ (no shad) (nb)	σ (EKS98) (nb)
	Pbp (5.5 TeV)		pPb (5.5 TeV)	
$y < 2.4$	8.23	8.37	8.12	7.39
$y < 1$	3.53	3.53	3.52	3.33
$2.4 < y < 4$	2.14	2.06	2.01	1.68
	Pbp (8.8 TeV)		pPb (8.8 TeV)	
$y < 2.4$	12.37	12.47	12.26	10.93
$y < 1$	5.22	5.11	5.20	4.82
$2.4 < y < 4$	5.07	5.03	4.83	3.95

Table 1: Z^0 cross sections per nucleon pair. No decay channel is specified.

Shadowing Effects on Dilepton Continuum

Drell-Yan production used as a reference process for quarkonium production at the CERN SPS

At higher energies, continuum extends to much higher masses

We show the effects of shadowing on dilepton production for $m > 4$ GeV as a function of mass and rapidity

Problem: Most of the continuum is not Drell-Yan like and is subject to other effects, as we will see

Shadowing in Lepton Pair Production

Production of a lepton pair with mass m at scale Q at next-to-leading order

$$\begin{aligned} \frac{1}{AB} \frac{d\sigma_{AB}^m}{dyd^2bd^2r} &= \int dz dz' dx_1 dx_2 dx \delta\left(\frac{m^2}{s} - xx_1x_2\right) \delta\left(y - \frac{1}{2} \ln\left(\frac{x_1}{x_2}\right)\right) \\ &\times \left\{ \sum_{i,j \in Q, \bar{Q}} H_{ij}^m C^{ii}(q_i, \bar{q}_j) \Delta_{q\bar{q}}(x) F_{q_i}^A(x_1, Q^2, \vec{r}, z) F_{\bar{q}_j}^B(x_2, Q^2, \vec{b} - \vec{r}, z') \right. \\ &+ \sum_{i,k \in Q, \bar{Q}} H_{ij}^m C^{if}(q_i, q_k) \Delta_{qg}(x) \left[F_{q_i}^A(x_1, Q^2, \vec{r}, z) F_g^B(x_2, Q^2, \vec{b} - \vec{r}, z') \right. \\ &\left. \left. + F_g^A(x_1, Q^2, \vec{r}, z) F_{q_j}^B(x_2, Q^2, \vec{b} - \vec{r}, z') \right] \right\}, \end{aligned}$$

There are three contributions to continuum lepton pair production: virtual photon exchange, Z^0 exchange, and $\gamma^* - Z^0$ interference

$$\begin{aligned} H_{ij}^m &= H_{ij}^{\gamma^*} + H_{ij}^{\gamma^*-Z^0} + H_{ij}^{Z^0} \\ H_{ij}^{\gamma^*} &= \frac{4\pi\alpha^2}{9m^2s} |e_i|^2 \\ H_{ij}^{\gamma^*-Z^0} &= \frac{\alpha G_F m_Z^2}{9\sqrt{2}s} \frac{(1 - 4\sin^2\theta_W)(m^2 - m_Z^2)}{(m^2 - m_Z^2)^2 + m_Z^2\Gamma_Z^2} |e_i| (1 - 4|e_i| \sin^2\theta_W) \\ H_{ij}^{Z^0} &= \frac{1 G_F m^2}{3\sqrt{2}s} \frac{m_Z \Gamma_{Z \rightarrow l+l^-}}{(m^2 - m_Z^2)^2 + m_Z^2\Gamma_Z^2} (1 + (1 - 4|e_i| \sin^2\theta_W)^2) \\ \Gamma_{Z \rightarrow l+l^-} &= \frac{\alpha m_Z (1 + (1 - 4\sin^2\theta_W)^2)}{48 \sin^2\theta_W \cos^2\theta_W} \\ \Gamma_Z &= 2.492 \text{ GeV} \end{aligned}$$

Dilepton Production: Convolution of Shadowing Functions with Parton Densities

$$\begin{aligned}
& \sum_{i,j \in Q\bar{Q}} S^i(A, x_1) S^j(B, x_2) f_{q_i}^N(x_1, Q^2) f_{\bar{q}_j}^N(x_2, Q^2) C^{ii}(q_i, \bar{q}_j) H_{ij}^m \\
&= H_{uu}^m \left(S^u(A, x_1) S^{\bar{u}}(B, x_2) \left\{ Z_A f_u^p(x_1, Q^2) + N_A f_u^n(x_1, Q^2) \right\} \right. \\
&\quad \times \left. \left\{ Z_B f_{\bar{u}}^p(x_2, Q^2) + N_B f_{\bar{u}}^n(x_2, Q^2) \right\} + 2ABS^c(A, x_1) S^{\bar{c}}(B, x_2) f_c^p(x_1, Q^2) f_{\bar{c}}^p(x_2, Q^2) \right) \\
&\quad + H_{dd}^m \left(S^d(A, x_1) S^{\bar{d}}(B, x_2) \left\{ Z_A f_d^p(x_1, Q^2) + N_A f_d^n(x_1, Q^2) \right\} \right. \\
&\quad \times \left. \left\{ Z_B f_{\bar{d}}^p(x_2, Q^2) + N_B f_{\bar{d}}^n(x_2, Q^2) \right\} + 2ABS^s(A, x_1) S^{\bar{s}}(B, x_2) f_s^p(x_1, Q^2) f_{\bar{s}}^p(x_2, Q^2) \right) \\
&\quad + [x_1 \leftrightarrow x_2, A \leftrightarrow B] .
\end{aligned}$$

$$\begin{aligned}
& \sum_{i,k \in Q\bar{Q}} \left(S^i(A, x_1) S^g(B, x_2) f_{q_i}^N(x_1, Q^2) f_g^N(x_2, Q^2) + [x_1 \leftrightarrow x_2, A \leftrightarrow B] \right) C^{if}(q_i, q_k) H_{ij}^m \\
&= BS^g(B, x_2) f_g^p(x_2, Q^2) \times \left\{ H_{uu}^m \left(S^u(A, x_1) \left\{ Z_A f_u^p(x_1, Q^2) + N_A f_u^n(x_1, Q^2) \right\} \right. \right. \\
&\quad \left. \left. + S^{\bar{u}}(A, x_1) \left\{ Z_B f_{\bar{u}}^p(x_2, Q^2) + N_B f_{\bar{u}}^n(x_2, Q^2) \right\} + 2AS^c(A, x_1) f_c^p(x_1, Q^2) \right) \right. \\
&\quad \left. + H_{dd}^m \left(S^d(A, x_1) \left\{ Z_A f_d^p(x_1, Q^2) + N_A f_d^n(x_1, Q^2) \right\} \right. \right. \\
&\quad \left. \left. + S^{\bar{d}}(A, x_1) \left\{ Z_B f_{\bar{d}}^p(x_2, Q^2) + N_B f_{\bar{d}}^n(x_2, Q^2) \right\} + 2AS^s(A, x_1) f_s^p(x_1, Q^2) \right) \right\} \\
&\quad + [x_1 \leftrightarrow x_2, A \leftrightarrow B] .
\end{aligned}$$

Drell-Yan Mass Distributions

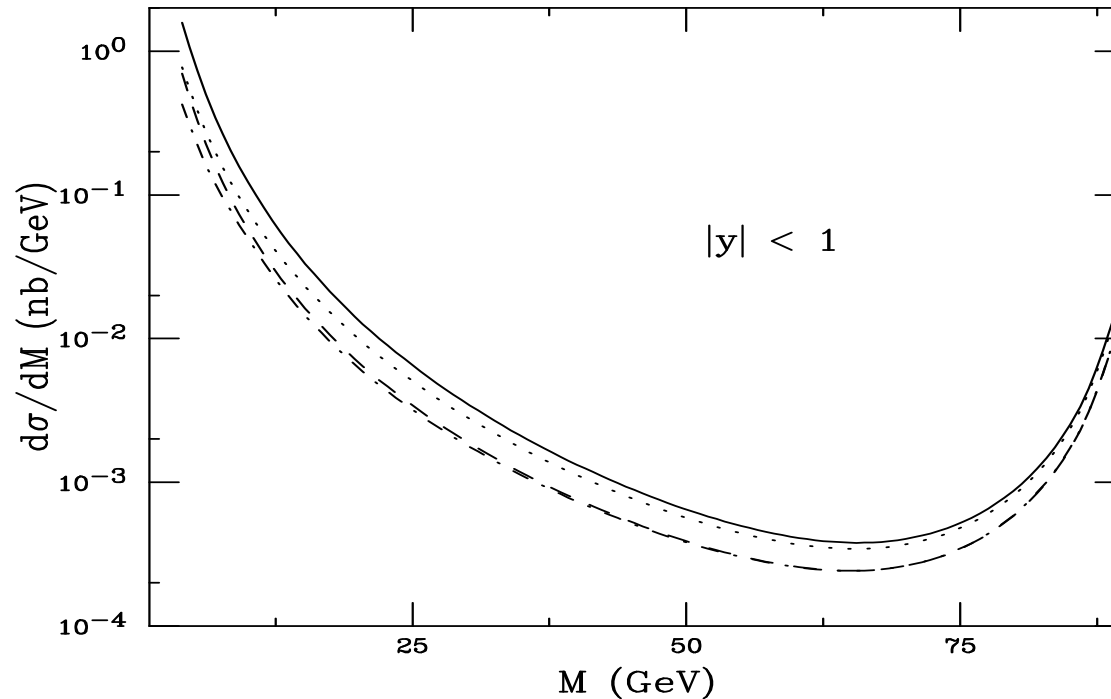


Figure 19: The mass distribution of dileptons in Pb+Pb collisions at 5.5 TeV in a rapidity window of $|y| < 1$. Contributions from γ^* , $\gamma^* - Z^0$ interference, and $Z^0 \rightarrow l^+l^-$ are included. We note that the interference and Z^0 decay contributions are a effect until $M > 40$ GeV. The solid curve is the distribution without shadowing. The homogeneous shadowing results are given in the dashed, HPC, dot-dashed, Eskola, and dotted, EKS98, lines.

Drell-Yan Shadowing vs. Mass

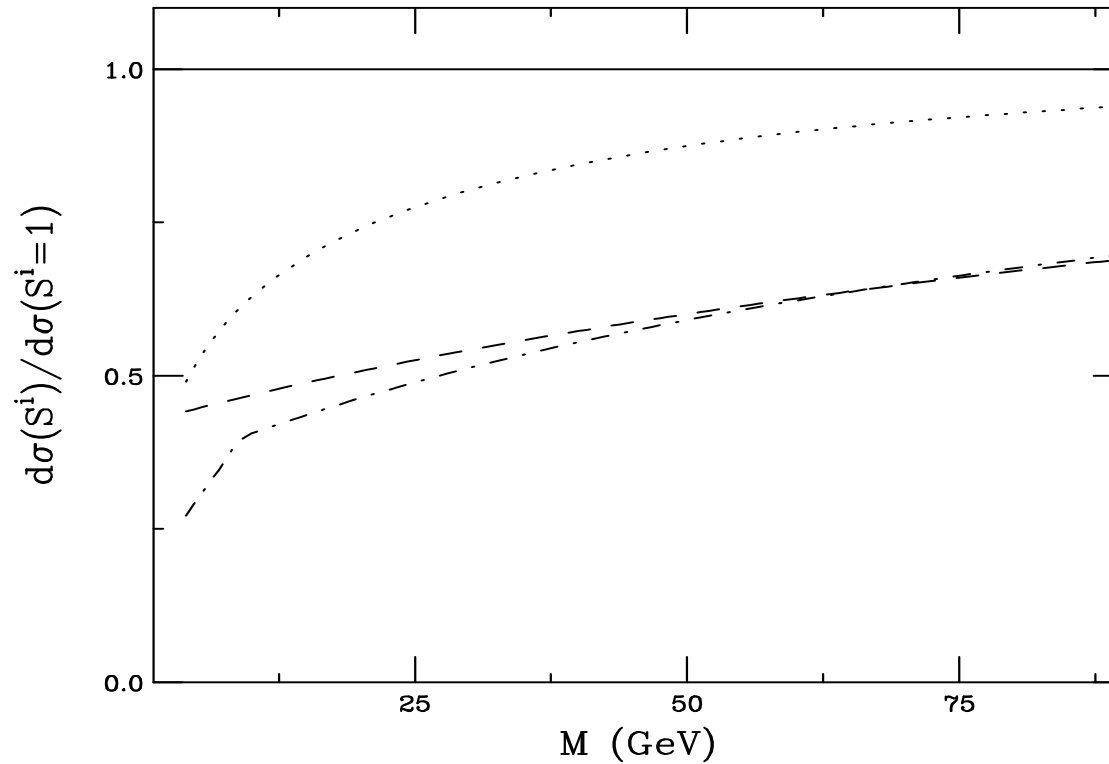


Figure 20: The ratio of dilepton production in Pb+Pb collisions at 5.5 TeV in a rapidity window of $|y| < 1$ with and without shadowing as a function of mass. The homogeneous shadowing results are given in the dashed, HPC, dot-dashed, Eskola, and dotted, EKS98, lines.

Drell-Yan K Factor vs. Mass

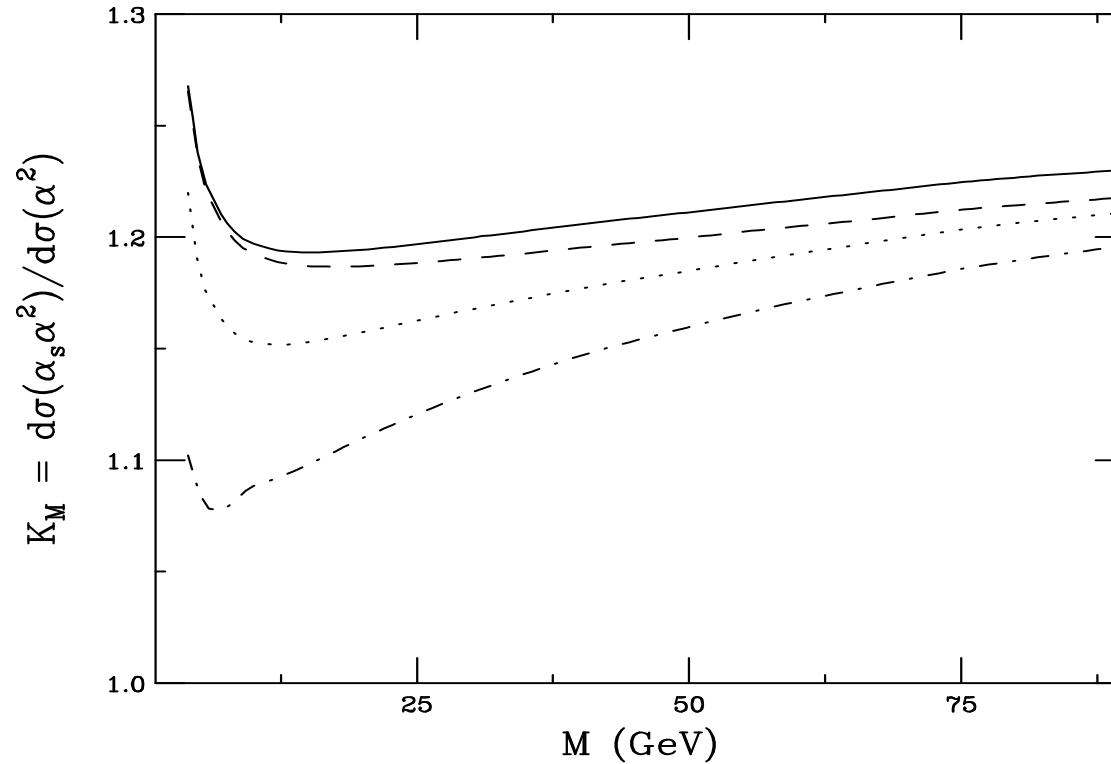


Figure 21: The NLO/LO ratio of dilepton production in Pb+Pb collisions at 5.5 TeV in a rapidity window of $|y| < 1$ as a function of mass. The solid curve is the K factor without shadowing. The homogeneous shadowing results are given in the dashed, HPC, dot-dashed, Eskola, and dotted, EKS98, lines.

Drell-Yan Shadowing vs. Rapidity in Mass Bins

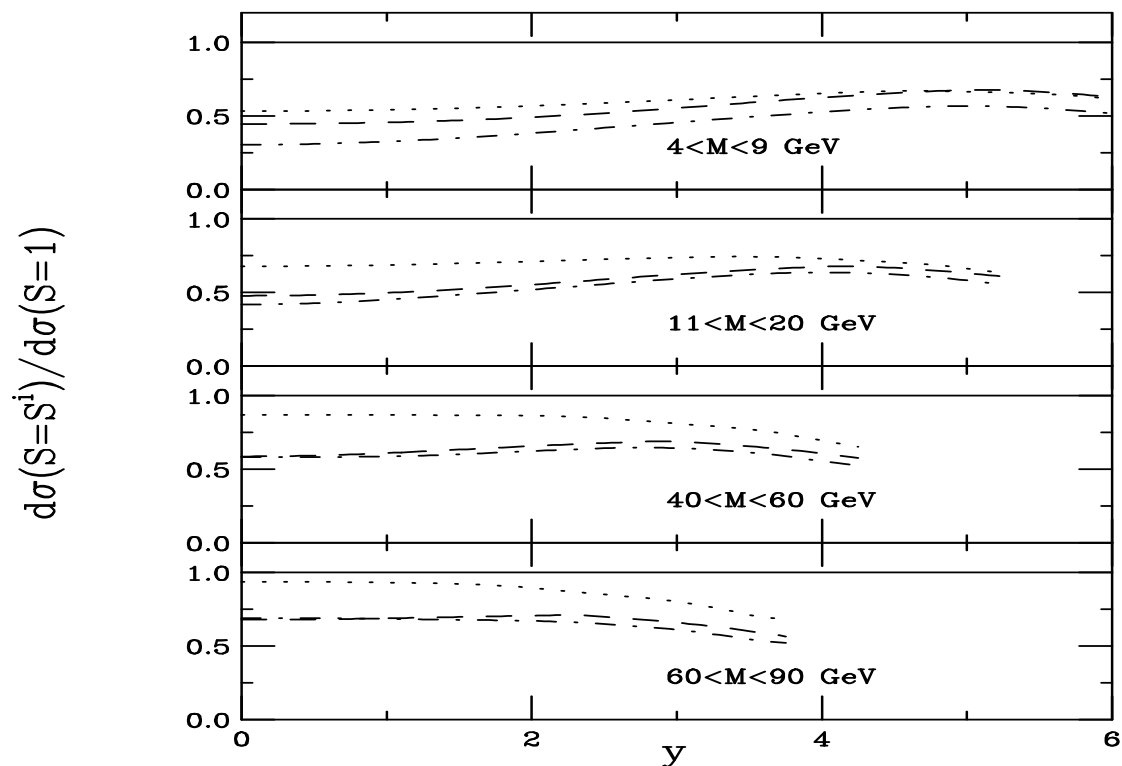


Figure 22: The ratio of dilepton production in Pb+Pb collisions at 5.5 TeV for $4 < M < 9$ GeV, $11 < M < 20$ GeV, $40 < M < 60$ GeV, and $60 < M < 90$ GeV with and without shadowing as a function of dilepton rapidity. The homogeneous shadowing results are given in the dashed, HPC, dot-dashed, Eskola, and dotted, EKS98, lines.

Drell-Yan K Factor vs. Rapidity

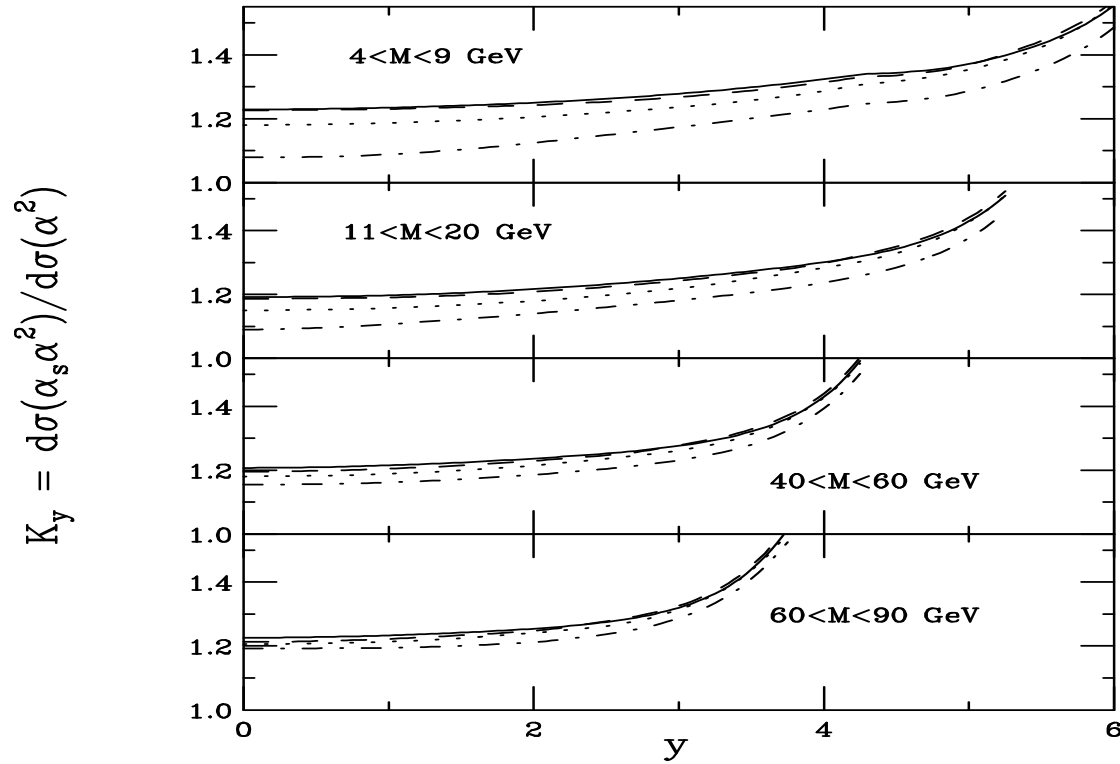


Figure 23: The NLO/LO ratio of dilepton production in Pb+Pb collisions at 5.5 TeV for $4 < M < 9$ GeV, $11 < M < 20$ GeV, $40 < M < 60$ GeV, and $60 < M < 90$ GeV as a function of rapidity. The solid curve is the K factor without shadowing. The homogeneous shadowing results are given in the dashed, HPC, dot-dashed, Eskola, and dotted, EKS98, lines.

Drell-Yan Rapidity Distributions in $p\text{Pb}$ and $\text{Pb}p$

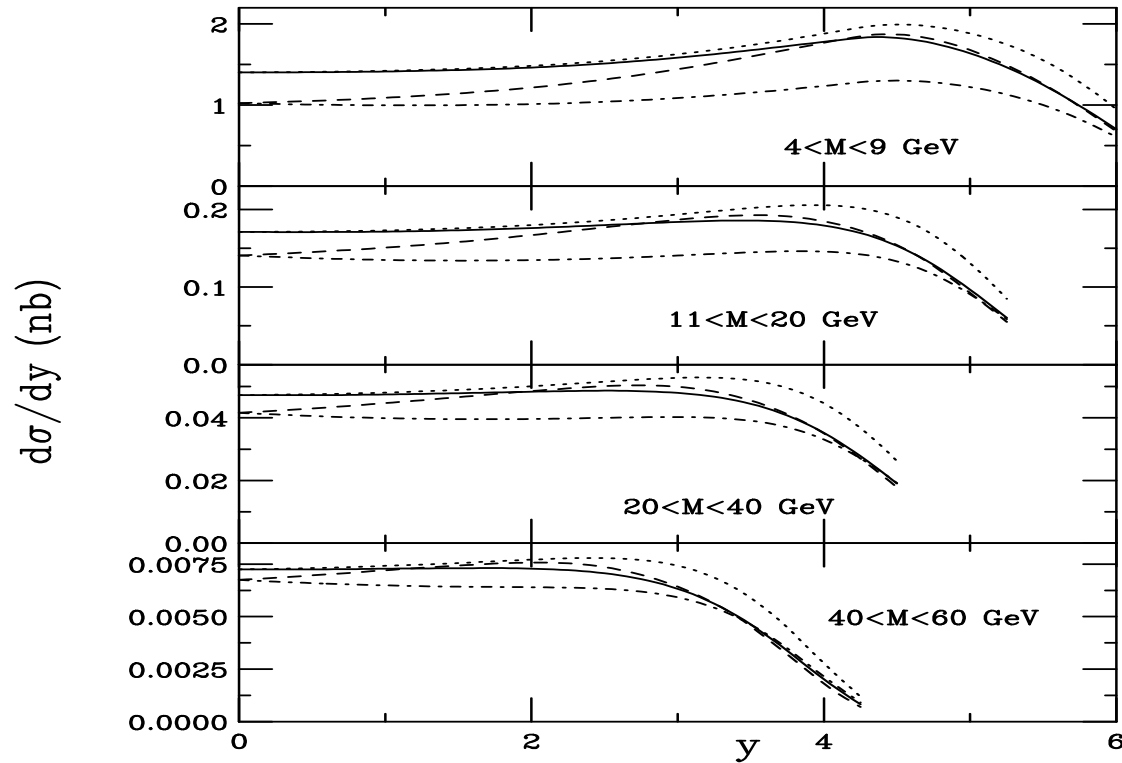


Figure 24: The Drell-Yan rapidity distributions in $p\text{Pb}$ and $\text{Pb}p$ collisions at 5.5 TeV evaluated at $Q = M$ for $4 < M < 9$ GeV, $11 < M < 20$ GeV, $20 < M < 40$ GeV and $40 < M < 60$ GeV. The solid and dashed curves show the results without and with shadowing respectively in $\text{Pb}p$ collisions while the dotted and dot-dashed curves give the results without and with shadowing for $p\text{Pb}$ collisions.

Drell-Yan Shadowing in $p\text{Pb}$ and $\text{Pb}p$

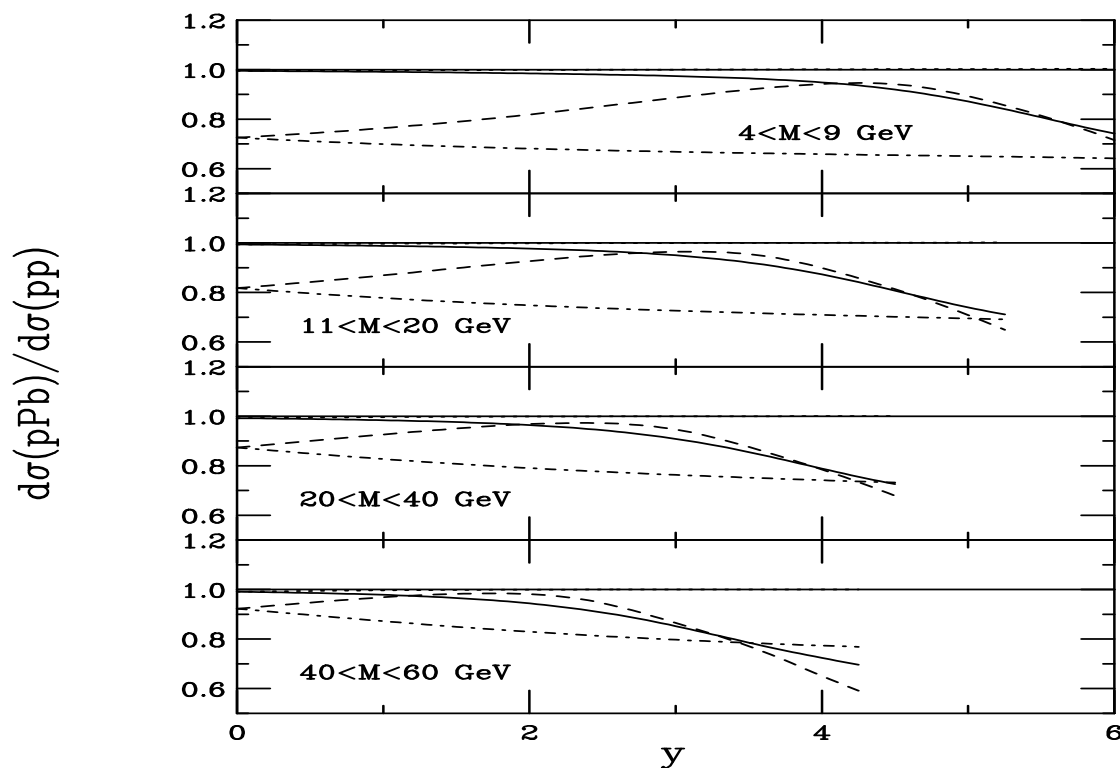


Figure 25: The ratios of $p\text{Pb}$ and $\text{Pb}p$ collisions to pp collisions at 5.5 TeV evaluated at $Q = M$ for $4 < M < 9 \text{ GeV}$, $11 < M < 20 \text{ GeV}$, $20 < M < 40 \text{ GeV}$ and $40 < M < 60 \text{ GeV}$, as a function of rapidity. The solid and dashed curves show the $\text{Pb}p/pp$ ratios without and with shadowing respectively while the dotted and dot-dashed curves are the $p\text{Pb}/pp$ ratios without and with shadowing.

Dependence on Scale and Shadowing Parameterization

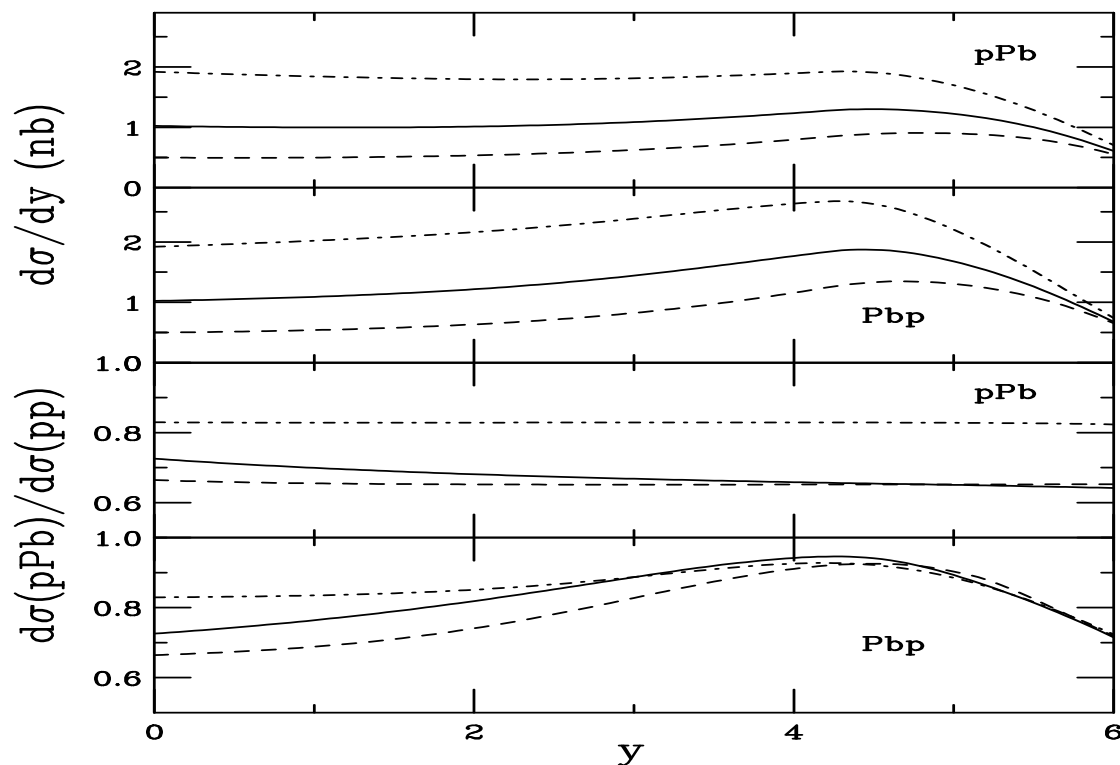


Figure 26: The upper 2 plots show scale dependence in $4 < M < 9$ GeV in pPb and Pbp collisions at 5.5 TeV with EKS98. The solid is $Q = M$, the dashed, $Q = M/2$, and the dot-dashed, $Q = 2M$. The lower 2 plots show the dependence on shadowing parameterization for pPb/pp and Pbp/pp at 5.5 TeV. The solid is EKS98, the dashed is HPC and the dot-dashed is HKM.

$b\bar{b}$ Biggest Contribution to Continuum Below the Z^0

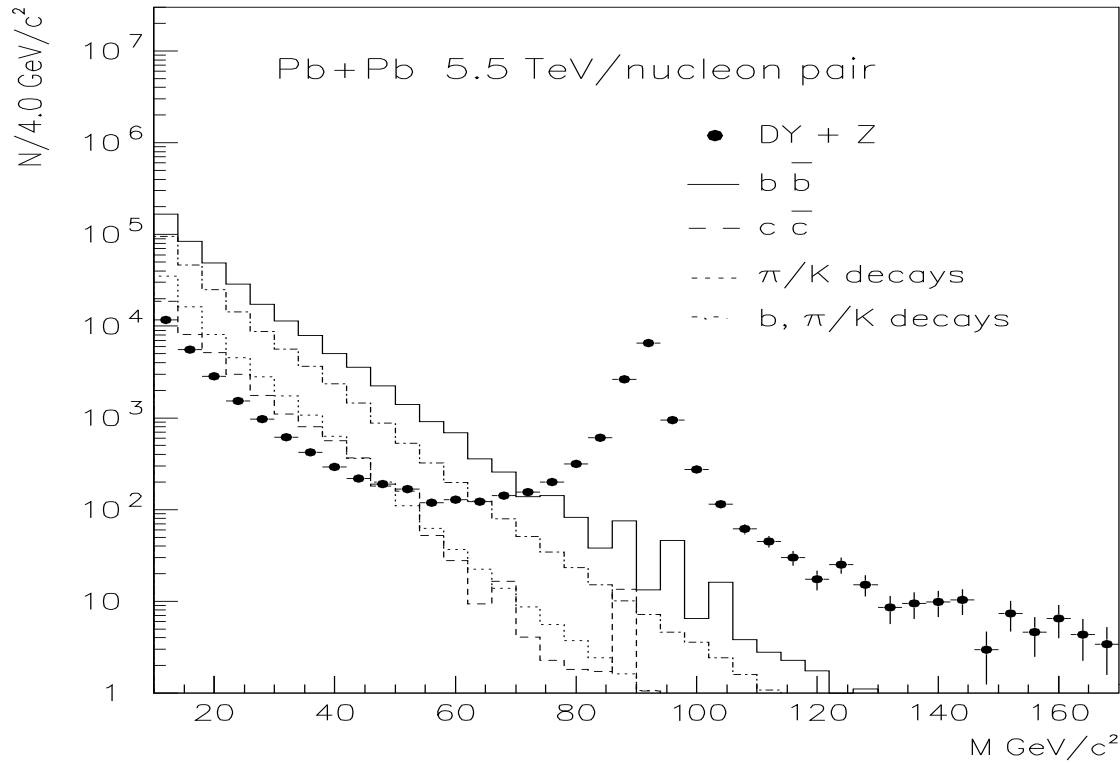


Figure 27: **Lepton pair invariant mass distributions above the Υ region with $p_T > 3.5 \text{ GeV}/c$. All major sources of background included. From ‘Heavy Ion Physics Programme in CMS’, CMS NOTE 2000/060.**

W^+ Production: Convolution of Shadowing Functions with Parton Densities

$q\bar{q} \rightarrow W^+ X$

$$\begin{aligned}
 & \sum_{i,j \in Q, \bar{Q}} S^i(A, x_1) S^j(B, x_2) f_{q_i}^N(x_1, Q^2) f_{\bar{q}_j}^N(x_2, Q^2) C^{\text{ii}}(q_i, \bar{q}_j) \\
 &= \cos^2 \theta_C \left(S^u(A, x_1) S^{\bar{d}}(B, x_2) \{ Z_A f_u^p(x_1, Q^2) + N_A f_u^n(x_1, Q^2) \} \right. \\
 & \times \{ Z_B f_d^p(x_2, Q^2) + N_B f_d^n(x_2, Q^2) \} + A B S^{\bar{s}}(A, x_1) S^c(B, x_2) f_s^p(x_1, Q^2) f_c^p(x_2, Q^2) \\
 & + \sin^2 \theta_C \left(S^u(A, x_1) S^{\bar{s}}(B, x_2) \{ Z_A f_u^p(x_1, Q^2) + N_A f_u^n(x_1, Q^2) \} B f_s^p(x_2, Q^2) \right. \\
 & \left. \left. + S^{\bar{d}}(A, x_1) S^c(B, x_2) \{ Z_A f_d^p(x_1, Q^2) + N_A f_d^n(x_1, Q^2) \} B f_c^p(x_2, Q^2) \right) \right) \\
 & + [x_1 \leftrightarrow x_2, A \leftrightarrow B] .
 \end{aligned}$$

$q(\bar{q})g \rightarrow W^+ X$

$$\begin{aligned}
 & \sum_{i,k \in Q, \bar{Q}} \left(S^i(A, x_1) S^g(B, x_2) f_{q_i}^N(x_1, Q^2) f_g^N(x_2, Q^2) + [x_1 \leftrightarrow x_2, A \leftrightarrow B] \right) C^{\text{if}}(q_i, q_k) \\
 &= B S^g(B, x_2) f_g^p(x_2, Q^2) \left[S^u(A, x_1) \{ Z_A f_u^p(x_1, Q^2) + N_A f_u^n(x_1, Q^2) \} \right. \\
 & \left. + S^{\bar{d}}(A, x_1) \{ Z_B f_d^p(x_2, Q^2) + N_B f_d^n(x_2, Q^2) \} + A \{ S^{\bar{s}}(A, x_1) f_s^p(x_1, Q^2) + S^c(A, x_1) f_c^p(x_1, Q^2) \} \right] \\
 & + [x_1 \leftrightarrow x_2, A \leftrightarrow B] .
 \end{aligned}$$

W^+ Distributions in pp Collisions at 5.5 and 14 TeV

pp cross sections increase with y due to dominance of $u_p(x_1)\bar{d}_p(x_2)$ contribution, $u_{Vp}(x_1)$ goes up with x_1 while $\bar{d}_p(x_2)$ goes up when x_2 decreases, peak at same point as in u_V distribution

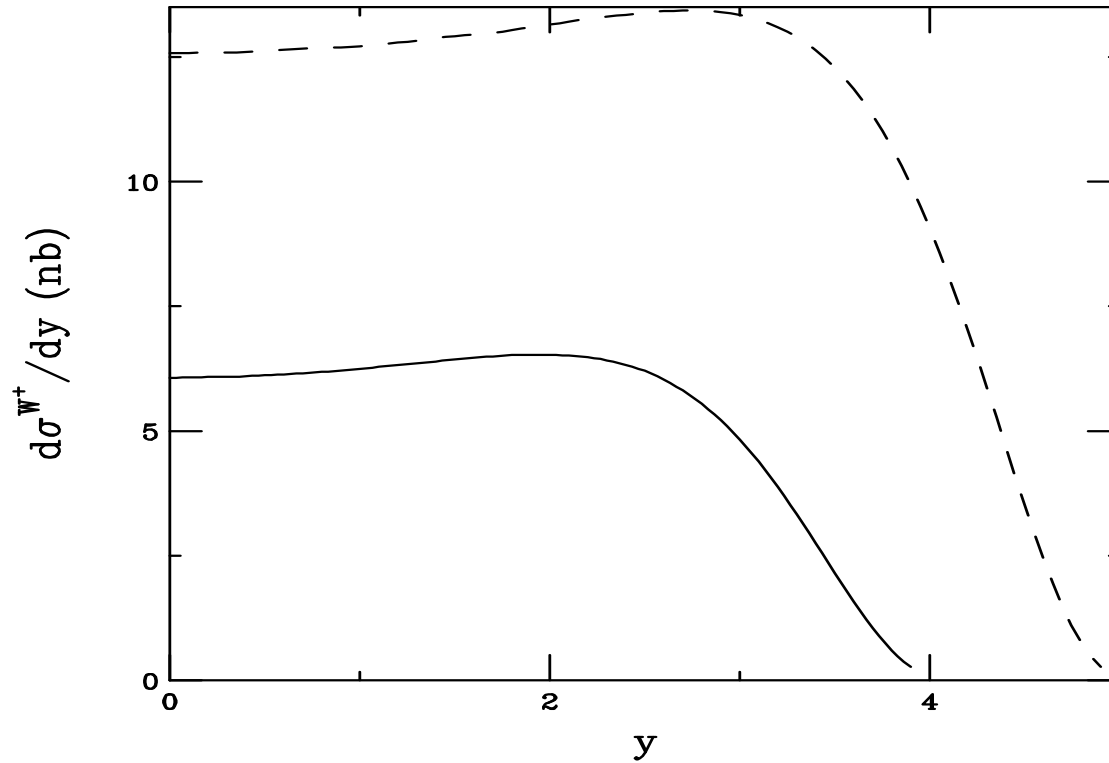


Figure 28: The W^+ rapidity distributions in pp collisions at 5.5 (solid) and 14 TeV (dashed), calculated with the MRST HO distributions.

W^+ Distributions in Pb+Pb Collisions at 5.5 TeV

Isospin washes out rise with rapidity in Pb+Pb

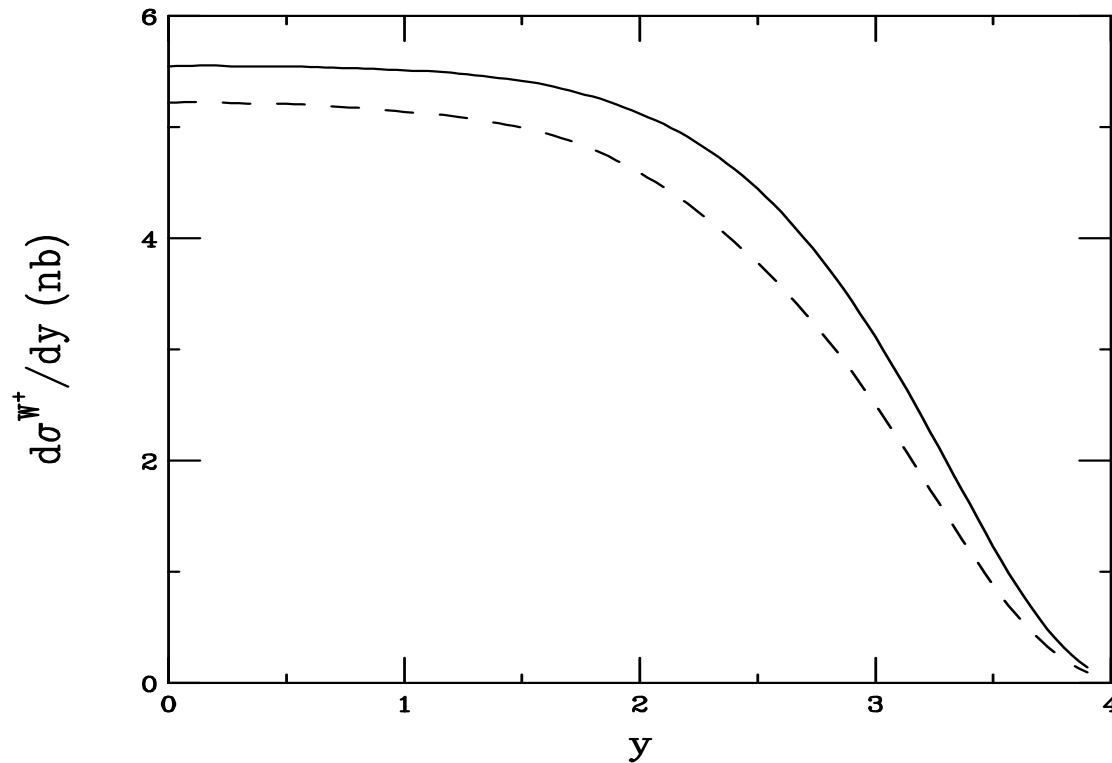


Figure 29: The W^+ rapidity distributions in Pb+Pb collisions at 5.5 TeV, without (solid) and with EKS98 shadowing (dashed), calculated with the MRST HO distributions.

W^+ Distributions in Pbp and pPb Collisions at 5.5 TeV

Pbp neutron excess wipes out rise with y

pPb , $(N/A)d_p(x_1)\bar{d}_p(x_2)$ enhances pA because $\bar{d} > \bar{u}$

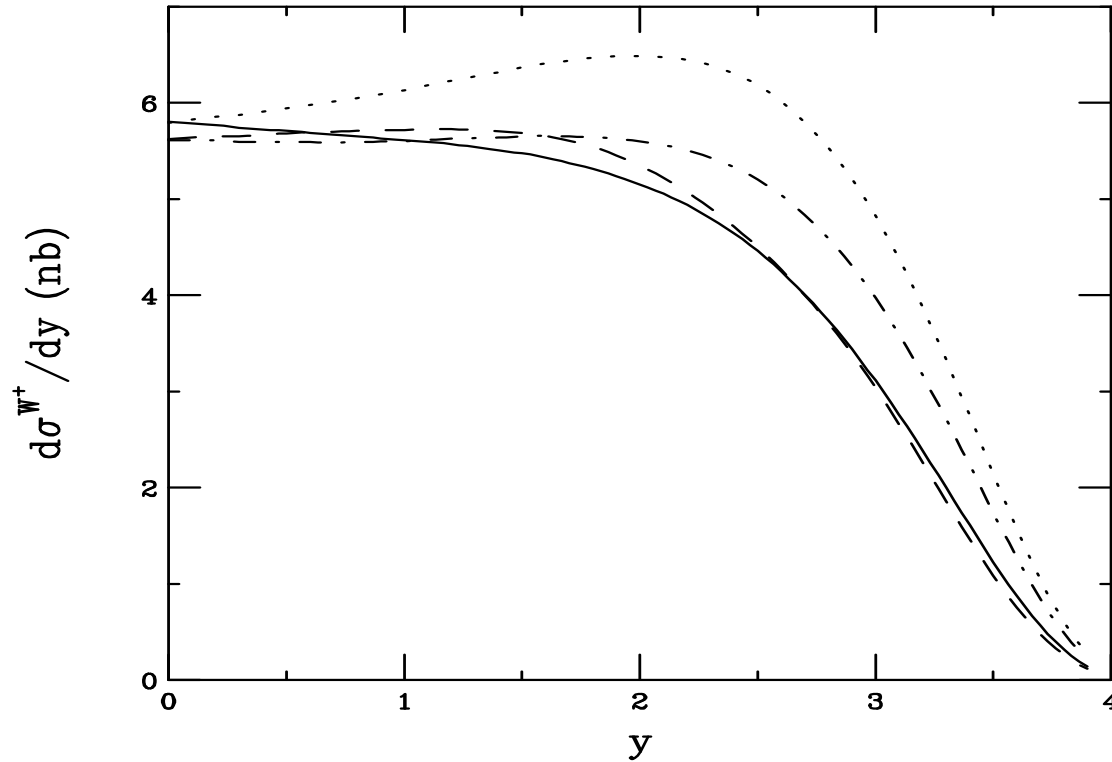


Figure 30: The W^+ rapidity distributions in Pbp and pPb collisions at 5.5 TeV, calculated with the MRST HO distributions. The solid and dashed curves show the results without and with shadowing respectively with the Pb nucleus coming from the left. The dotted and dash-dotted curves give the results without and with shadowing for the proton coming from the left.

Shadowing Effects on W^+ Production in Pbp and pPb Collisions at 5.5 TeV

In Pbp collisions, x_1 is in nucleus, x_1 increases with y into antishadowing and Fermi motion region, ratio increases

In pPb collisions, x_2 in nucleus, goes into shadowing region, ratio decreases

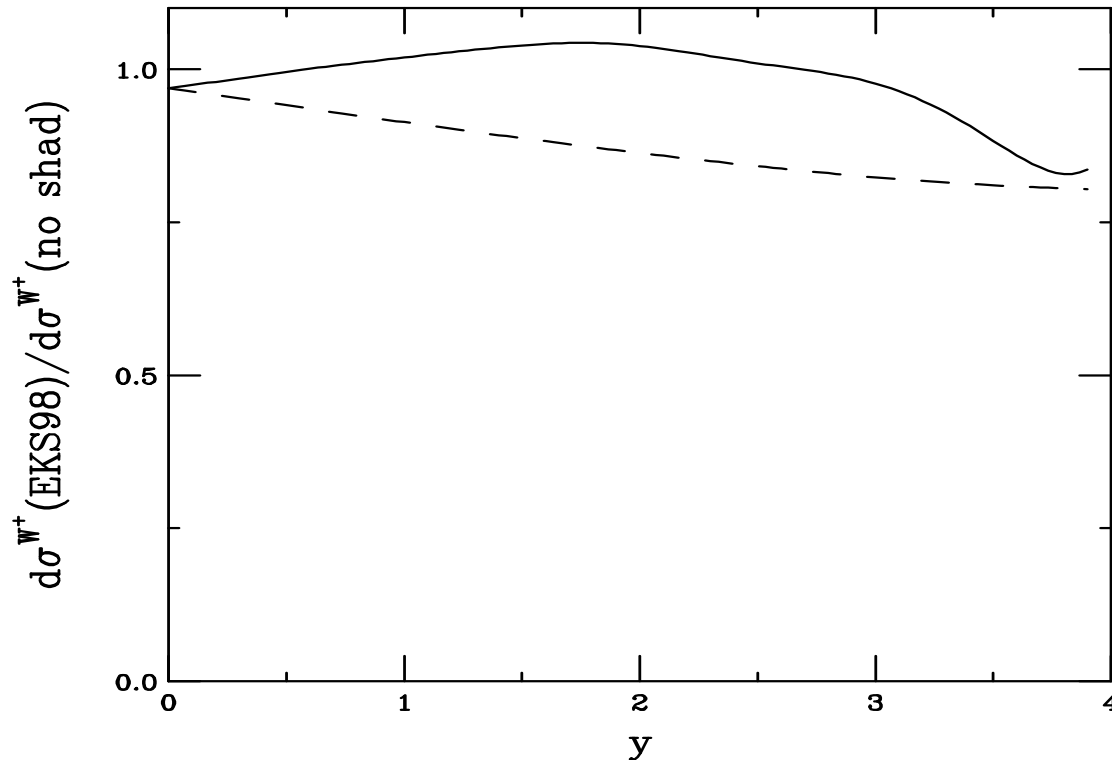


Figure 31: Ratios of shadowed to unshadowed W^+ rapidity distributions in Pbp (solid) and pPb (dashed) collisions at 5.5 TeV.

W^+ Production Ratios Pbp/pp and pPb/pp at 5.5 TeV

Neutron excess depletes Pbp/pp

pPb/pp without shadowing shows a rise due to extra neutrons in Pb (x_2)

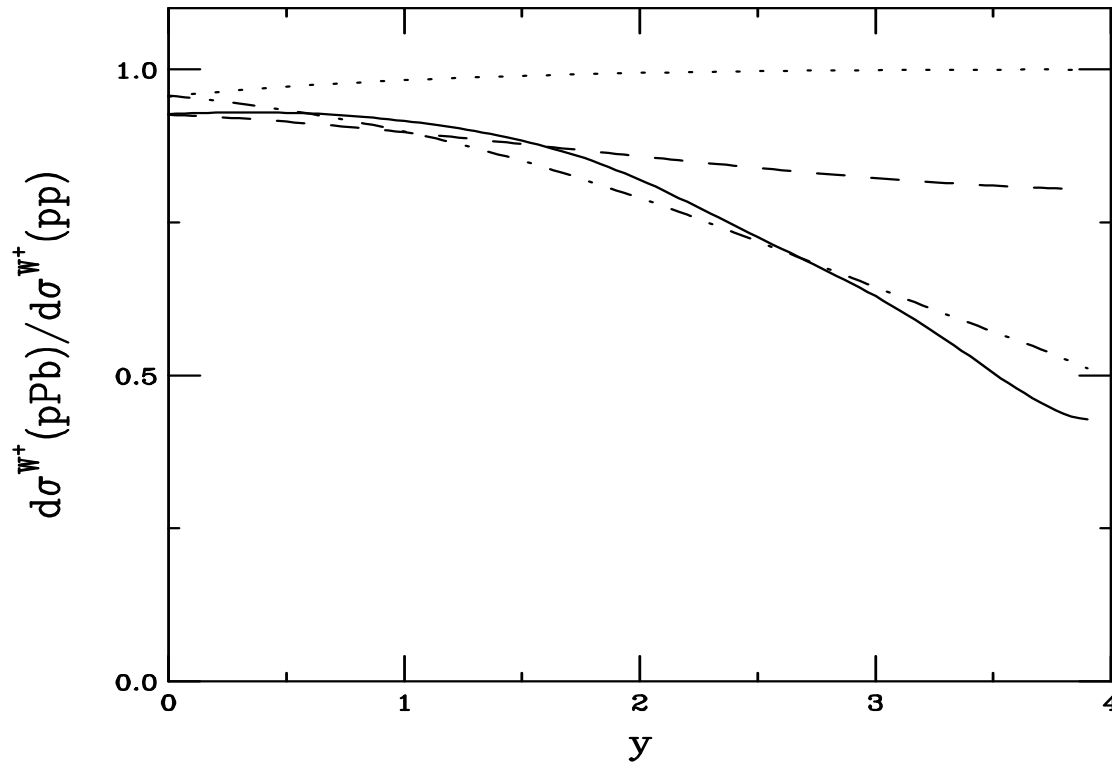


Figure 32: The ratios of Pbp/pp with (solid) and without (dot-dashed) shadowing and pPb/pp with (dashed) and without (dotted) shadowing at 5.5 TeV.

W^+ Cross Sections

Rapidity	σ (nb)	σ (nb)	σ (no shad) (nb)	σ (EKS98) (nb)
	<i>pp</i> (14 TeV)	<i>pp</i> (5.5 TeV)	Pb+Pb (5.5 TeV)	
$y < 2.4$	30.85	15.13	12.88	11.86
$y < 1$	12.63	6.13	5.54	5.20
$2.4 < y < 4$	19.97	5.68	3.71	2.99

Rapidity	σ (no shad) (nb)	σ (EKS98) (nb)	σ (no shad) (nb)	σ (EKS98) (nb)
	Pbp (5.5 TeV)		<i>p</i> Pb (5.5 TeV)	
$y < 2.4$	13.12	13.34	14.87	13.43
$y < 1$	5.71	5.67	5.95	5.60
$2.4 < y < 4$	3.72	3.62	5.67	4.69
	Pbp (8.8 TeV)		<i>p</i> Pb (8.8 TeV)	
$y < 2.4$	19.62	19.71	21.41	18.96
$y < 1$	8.37	8.16	8.60	7.92
$2.4 < y < 4$	8.30	8.31	11.80	9.58

Table 2: W^+ cross sections per nucleon pair. No decay channel is specified.

W⁻ Production: Convolution of Shadowing Functions with Parton Densities

$q\bar{q} \rightarrow W^- X$

$$\begin{aligned}
 & \sum_{i,j \in Q\bar{Q}} S^i(A, x_1) S^j(B, x_2) f_{q_i}^N(x_1, Q^2) f_{\bar{q}_j}^N(x_2, Q^2) C^{ii}(q_i, \bar{q}_j) \\
 &= \cos^2 \theta_C \left(S^{\bar{u}}(A, x_1) S^d(B, x_2) \{ Z_A f_u^p(x_1, Q^2) + N_A f_u^n(x_1, Q^2) \} \right. \\
 & \times \{ Z_B f_d^p(x_2, Q^2) + N_B f_d^n(x_2, Q^2) \} + A B S^s(A, x_1) S^{\bar{c}}(B, x_2) f_s^p(x_1, Q^2) f_{\bar{c}}^p(x_2, Q^2) \\
 & + \sin^2 \theta_C \left(S^{\bar{u}}(A, x_1) S^s(B, x_2) \{ Z_A f_u^p(x_1, Q^2) + N_A f_u^n(x_1, Q^2) \} B f_s^p(x_2, Q^2) \right. \\
 & \left. + S^d(A, x_1) S^{\bar{c}}(B, x_2) \{ Z_A f_d^p(x_1, Q^2) + N_A f_d^n(x_1, Q^2) \} B f_{\bar{c}}^p(x_2, Q^2) \right) \\
 & + [x_1 \leftrightarrow x_2, A \leftrightarrow B] .
 \end{aligned}$$

$q(\bar{q})g \rightarrow W^- X$

$$\begin{aligned}
 & \sum_{i,k \in Q\bar{Q}} \left(S^i(A, x_1) S^g(B, x_2) f_{q_i}^N(x_1, Q^2) f_g^N(x_2, Q^2) + [x_1 \leftrightarrow x_2, A \leftrightarrow B] \right) C^{if}(q_i, q_k) \\
 &= B S^g(B, x_2) f_g^p(x_2, Q^2) \left[S^{\bar{u}}(A, x_1) \{ Z_A f_u^p(x_1, Q^2) + N_A f_u^n(x_1, Q^2) \} \right. \\
 & \left. + S^d(A, x_1) \{ Z_B f_d^p(x_2, Q^2) + N_B f_d^n(x_2, Q^2) \} + A \{ S^s(A, x_1) f_s^p(x_1, Q^2) + S^{\bar{c}}(A, x_1) f_{\bar{c}}^p(x_1, Q^2) \} \right] \\
 & + [x_1 \leftrightarrow x_2, A \leftrightarrow B] .
 \end{aligned}$$

W^- Distributions in pp Collisions at 5.5 and 14 TeV

W^- decreases with y because valence d has smaller x

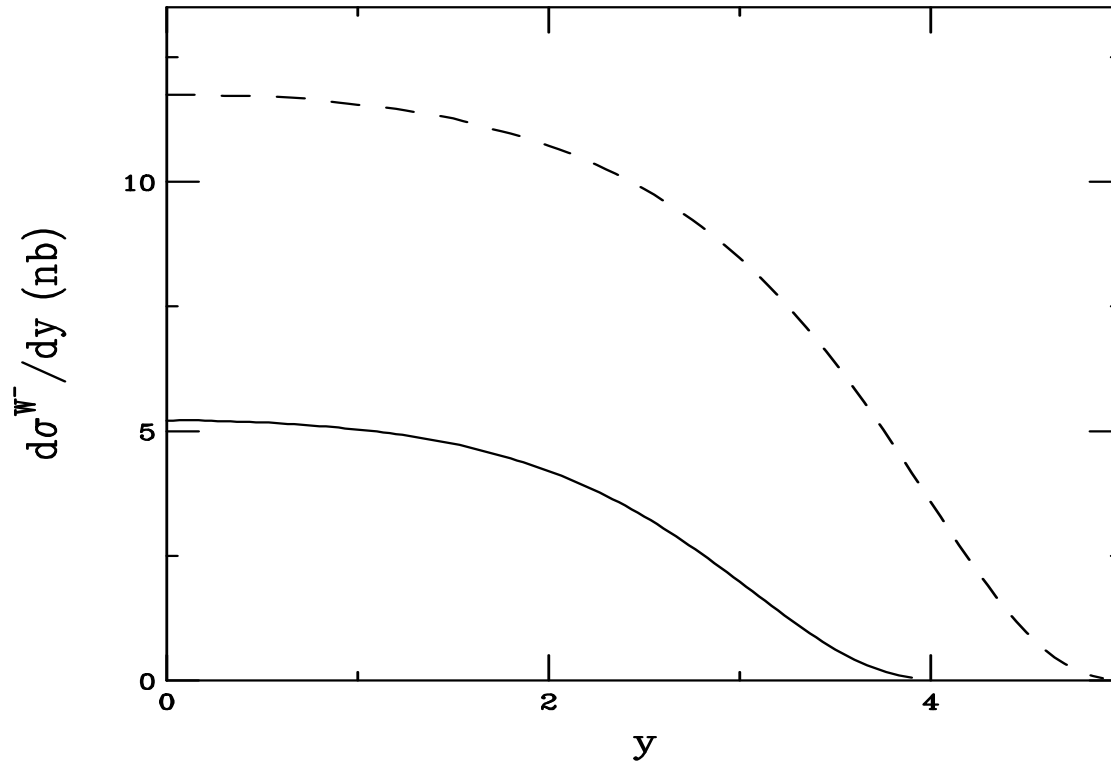


Figure 33: The W^- rapidity distributions in pp collisions at 5.5 (solid) and 14 TeV (dashed), calculated with the MRST HO distributions.

W^- Distributions in Pb+Pb Collisions at 5.5 TeV

Neutron excess of Pb causes flatter y distribution

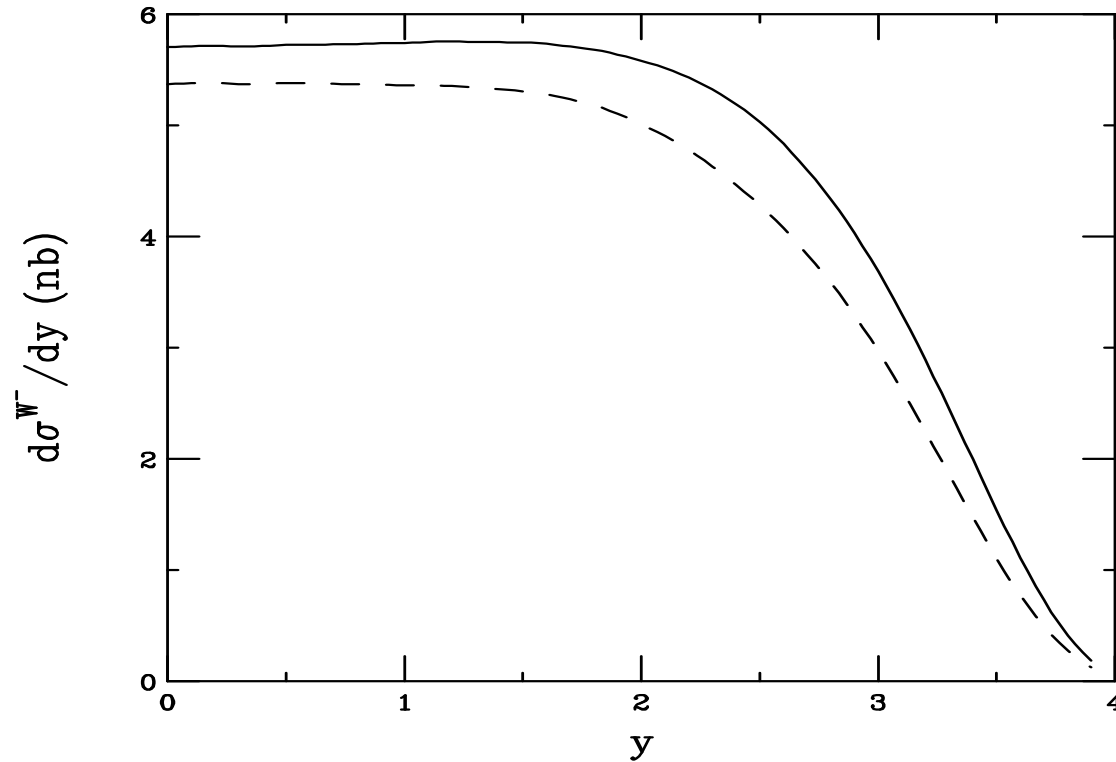


Figure 34: The W^- rapidity distributions in Pb+Pb collisions at 5.5 TeV, without (solid) and with EKS98 shadowing (dashed), calculated with the MRST HO distributions.

W^- Distributions in Pbp and pPb Collisions at 5.5 TeV

Neutron excess in Pb enhances Pbp at large y ($((N/A)u_p(x_1)\bar{u}_p(x_2))$)

pPb has smaller isospin effect

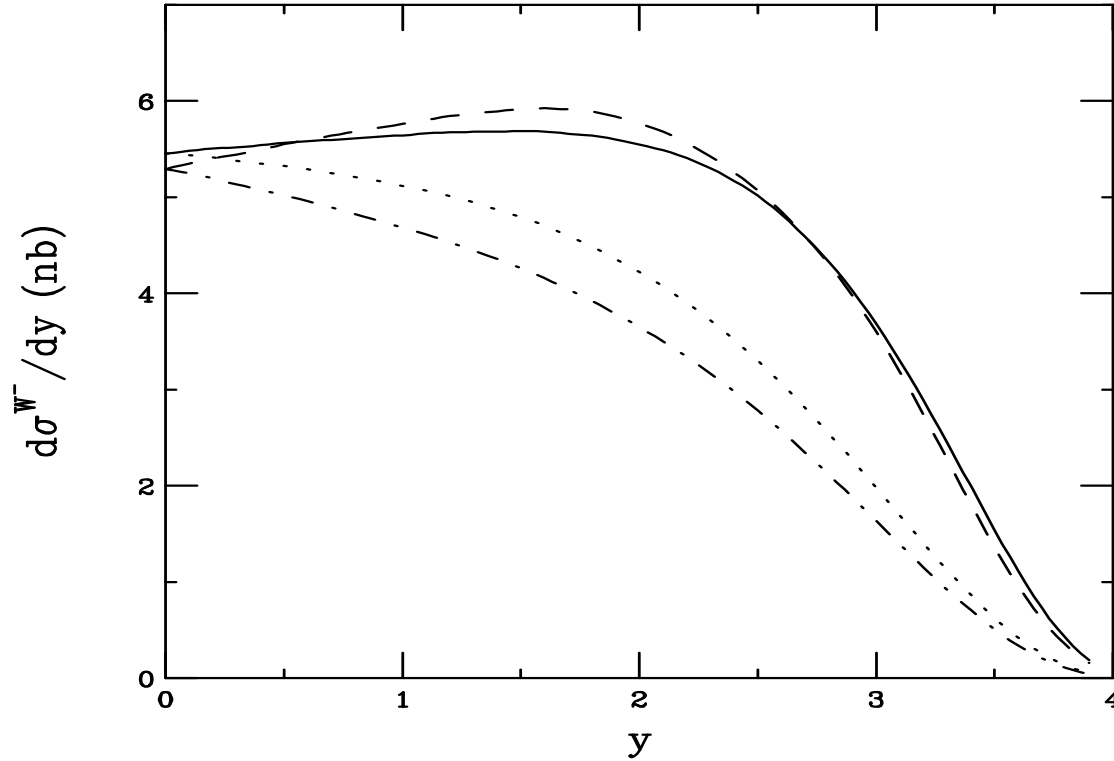


Figure 35: The W^- rapidity distributions in Pbp and pPb collisions at 5.5 TeV, calculated with the MRST HO distributions. The solid and dashed curves show the results without and with shadowing respectively with the Pb nucleus coming from the left. The dotted and dashed curves give the results without and with shadowing for the proton coming from the left.

Shadowing Effects on W^- Production in Pb p and p Pb Collisions at 5.5 TeV

In Pb p collisions, x_1 is in nucleus, x_1 increases with y into antishadowing and Fermi motion region, ratio increases

In p Pb collisions, x_2 in nucleus, goes into shadowing region, ratio decreases

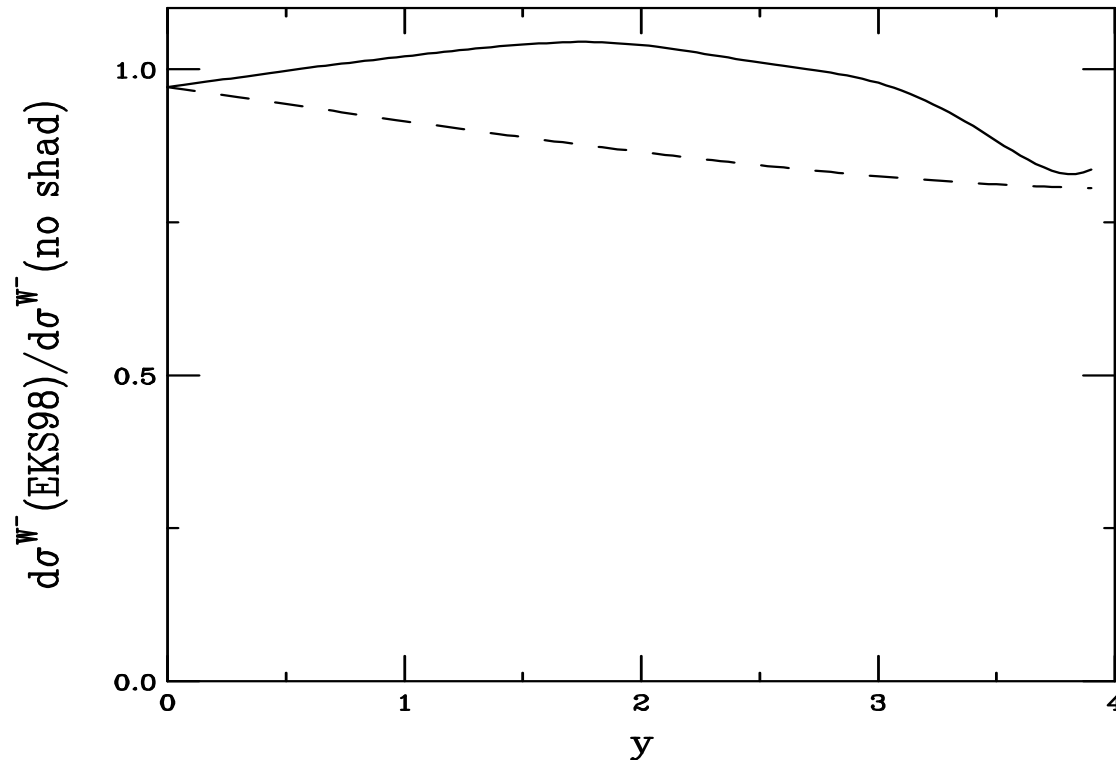


Figure 36: Ratios of shadowed to unshadowed W^- rapidity distributions in Pb p (solid) and p Pb (dashed) collisions at 5.5 TeV.

W^- Production Ratios Pbp/pp and pPb/pp at 5.5 TeV

Pbp/pp enhanced by neutron excess

pPb/pp shows small depletion with y

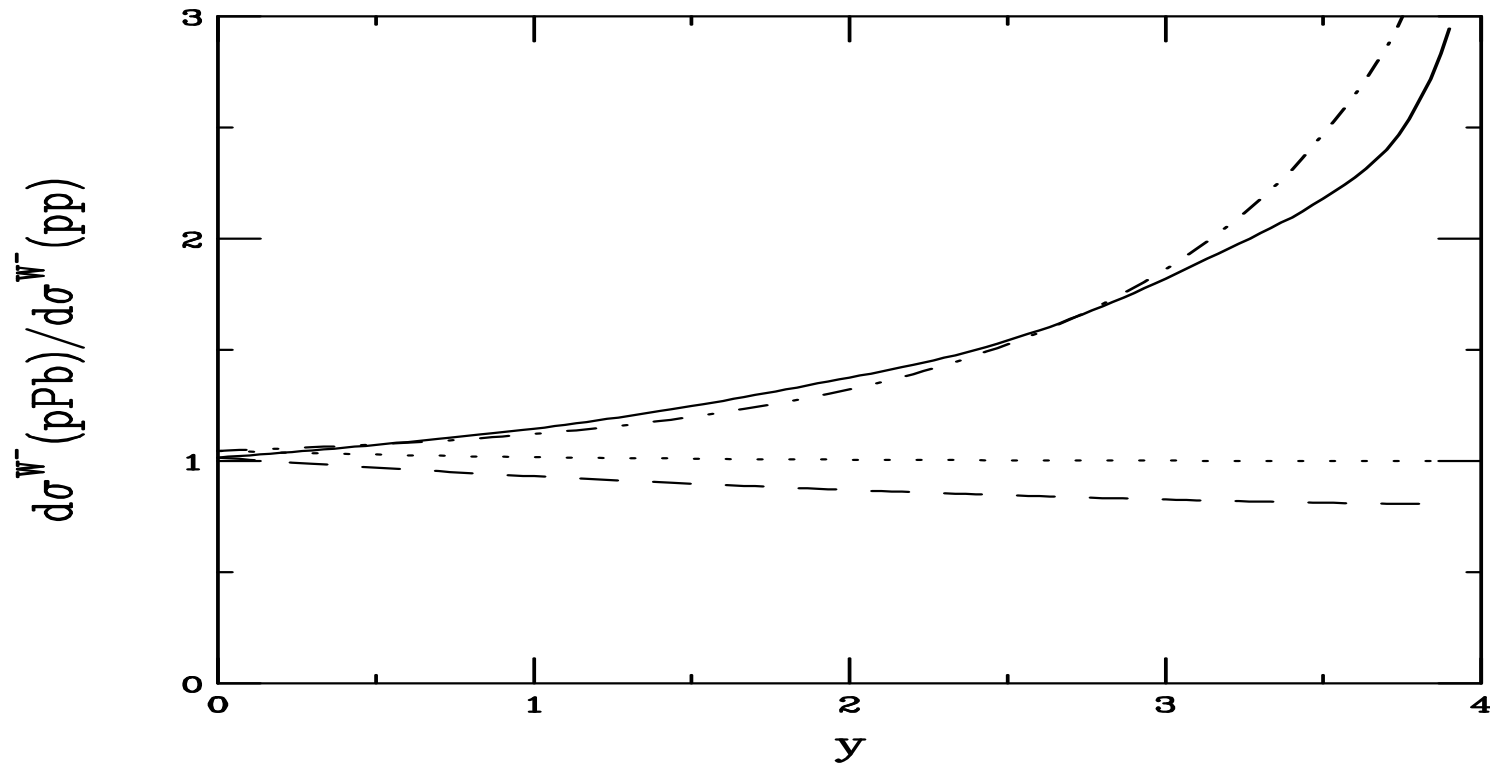


Figure 37: The ratios of Pbp/pp with (solid) and without (dot-dashed) shadowing and pPb/pp with (dashed) and without (dotted) shadowing at 5.5 TeV.

W^- Cross Sections at LHC

W^- Cross Sections

Rapidity	σ (nb)	σ (nb)	σ (no shad) (nb)	σ (EKS98) (nb)
	<i>pp</i> (14 TeV)	<i>pp</i> (5.5 TeV)	Pb+Pb (5.5 TeV)	
$y < 2.4$	27.07	11.41	13.61	12.55
$y < 1$	11.69	5.16	5.72	5.37
$2.4 < y < 4$	11.84	2.42	4.37	3.52

Rapidity	σ (no shad) (nb)	σ (EKS98) (nb)	σ (no shad) (nb)	σ (EKS98) (nb)
	Pbp (5.5 TeV)		pPb (5.5 TeV)	
$y < 2.4$	13.37	13.63	11.62	10.57
$y < 1$	5.56	5.54	5.31	5.01
$2.4 < y < 4$	4.36	4.24	2.43	2.02
	Pbp (8.8 TeV)		pPb (8.8 TeV)	
$y < 2.4$	19.87	20.01	18.08	16.09
$y < 1$	8.22	8.02	7.98	7.35
$2.4 < y < 4$	9.46	9.47	5.98	4.87

Table 3: W^- cross sections per nucleon pair. No decay channel is specified.

Similar Trends Seen for PbPb/pp Ratios

$$\text{PbPb}/pp \approx \text{Pbp}/pp \times p\text{Pb}/pp$$

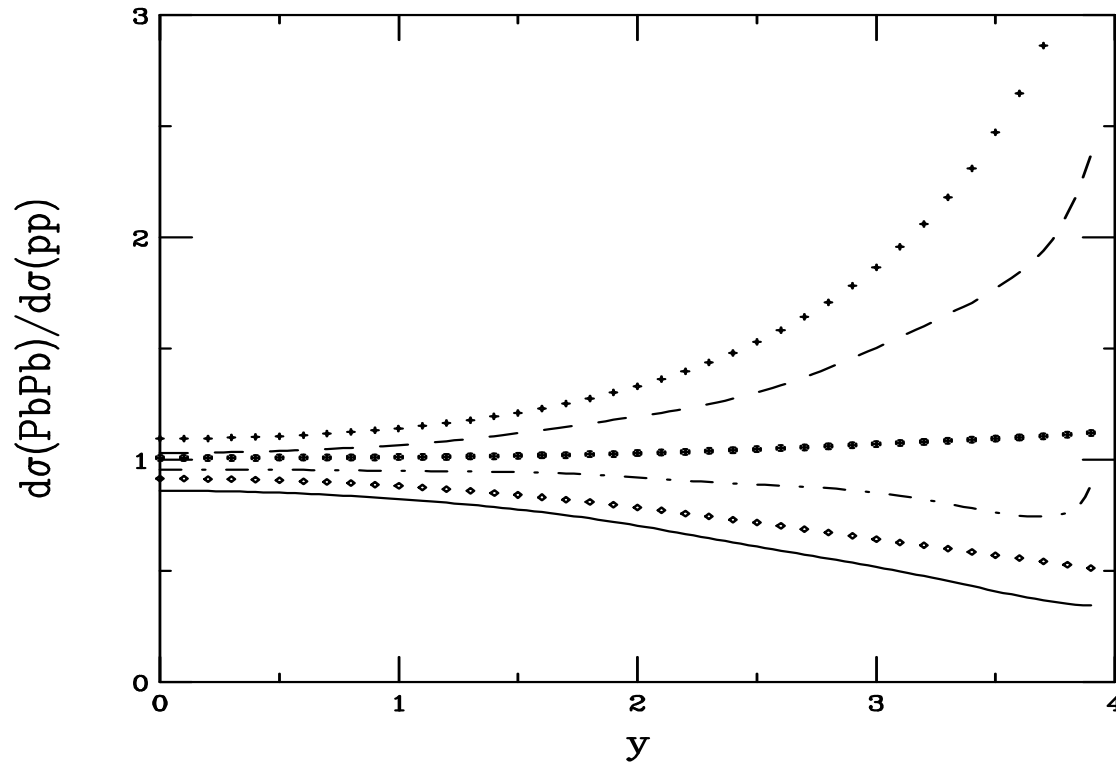


Figure 38: The ratios of PbPb/pp with (curves) and without (points) shadowing at 5.5 TeV. The curves are for W^+ (solid), W^- (dashed) and Z^0 (dot-dashed) while the points are W^+ (crosses), W^- (diamonds) and Z^0 (circles).

Conclusions

- Shadowing can play an important role in gauge boson production
- Gauge boson production a good probe of high Q^2 nuclear quark and antiquark distributions
- Changing scale affects shape of K factor but has a small effect on total cross sections
- Model dependence of shadowing is significant
- Scale dependence of shadowing is smaller effect
- Isospin effects are important in $q\bar{q}'$ dominated processes
- Production in Pb+Pb and p Pb should be compared to pp at 5.5 TeV where x values are the same and isospin contributions easier to identify
- High statistics studies preferable to discern properties of nuclear distributions at high Q^2